

AD/A-003 981

INVESTIGATION OF BASIC ELECTRONIC
TRANSPORT, RECOMBINATION AND OPTICAL
PROPERTIES IN $\text{InAs}_{1-x}\text{P}_x$ ALLOY SYSTEMS
AND THE GaSb EPITAXIAL FILMS FOR 1-2
MICROMETER IR APPLICATIONS

Sheng S. Li

Florida University

Prepared for:

Army Electronics Command
Advanced Research Projects Agency

15 June 1974

DISTRIBUTED BY:

NTIS

National Technical Information Service
U. S. DEPARTMENT OF COMMERCE

Unclassified
Security Classification

AD/A - 003981

DOCUMENT CONTROL DATA - R&D		
(Security classification of title, body of abstract and indexing annotation must be entered when the overall report is classified)		
1. ORIGINATING ACTIVITY (Corporate author) University of Florida Engineering and Industrial Experiment Station Gainesville, Florida 32601		2a. REPORT SECURITY CLASSIFICATION Unclassified
		2b. GROUP
3. REPORT TITLE Investigation of Basic Electronic Transport, Recombination and Optical Properties in $\text{InAs}_{1-x}\text{P}_x$ Alloy Systems and the GaSb Epitaxial Films for 1-2 μm IR Applications		
4. DESCRIPTIVE NOTES (Type of report and inclusive dates) First Semi-Annual Technical Report, 1 Dec. 1973 - 31, May 1974		
5. AUTHOR(S) (First name, middle initial, last name) Sheng S. Li		
6. REPORT DATE 15, June, 1974	7a. TOTAL NO. OF PAGES 84	7b. NO. OF REFS 20
8a. CONTRACT OR GRANT NO. DAAK02-74-C-0102	9a. ORIGINATOR'S REPORT NUMBER(S) Progress Report No. 1	
a. PROJECT, TASK, WORK UNIT NOS. 2182, n/a, n/a		
c. DOD ELEMENT 4D10		
d. DOD SUBELEMENT	9b. OTHER REPORT NO(S) (Any other numbers that may be assigned this report)	
10. DISTRIBUTION STATEMENT OF THIS REPORT [REDACTED]		
11. SUPPLEMENTARY NOTES This research was supported by the Defense Advanced Research Project Agency.		12. SPONSORING MILITARY ACTIVITY Night Vision Laboratory U.S. Army Electronics Command Fort Belvoir, Virginia 22060
13. ABSTRACT A systematic study has been made on the effect of hydrogen carrier gas flow-rate on the electron concentration and electron mobility of the epitaxially grown $\text{InAs}_{0.61}\text{P}_{0.39}$ samples. Resistivity and Hall effect measurements yield the resistivity, Hall coefficient, electron mobility and electron density as a function of temperature between 3°K and 300°K for epitaxial samples 153 to 159 and the bulk samples H-2, H-5 and H-6. The activation energy for the donor states, the density of donors and acceptors and scattering mechanisms for electrons in $\text{InAs}_{1-x}\text{P}_x$ alloys were calculated and analyzed. The alloy compositions were determined from the electron microprobe analysis. The energy band gap versus alloy composition for the $\text{InAs}_{1-x}\text{P}_x$ system was deduced from the optical transmission data. Optical absorption coefficients near the fundamental absorption edge were obtained for bulk samples H-1, H-2, H-5, H-6, H-7 and W16. The result shows that the energy band gap varies linearly with the alloy composition in $\text{InAs}_{1-x}\text{P}_x$.		

Reproduced by
NATIONAL TECHNICAL
INFORMATION SERVICE
US Department of Commerce
Springfield, VA. 22151

PRICES SUBJECT TO CHANGE

DD FORM 1473
1 NOV 65

Unclassified
Security Classification

Unclassified

Security Classification

14. KEY WORDS	LINK A		LINK B		LINK C	
	ROLE	WT	ROLE	WT	ROLE	WT
InAs _{1-x} P _x						
Resistivity						
Hall coefficient						
Electron mobility						
Absorption coefficient						
Scattering mechanisms						
Energy band gap						
Activation energy of donors states						
Impurity hopping conduction						

Unclassified

Security Classification

FOREWORD

This report covers the research activities between December 1973 and May 1974 under contract DAAK02-74-C-0102. Mr. David Jackson (AMSEL-NV-II) is the responsible Army Night Vision contract monitor. The work was executed by the Department of Electrical Engineering of the University of Florida. The principal investigator of this project is Dr. Sheng S. Li. Major contributors are Mr. J. Anderson, Mr. D. Schoenfeld and Mr. R. Owen. Additional support was derived, during the reporting period from Dr. J. Kennedy of Air Force Cambridge Research Laboratories who generously prepared the $\text{InAs}_{1-x}\text{P}_x$ epitaxial films for this contract research. We acknowledge the receipt of the bulk $\text{InAs}_{1-x}\text{P}_x$ samples from Dr. R. Behringer of Naval Research Laboratories.

ABSTRACT

The research program sponsored by this contract during the first six months has produced technical findings in several areas: (1) A systematic study has been made on the effect of the hydrogen carrier gas flow-rate on the electron concentration and electron mobility of seven (153-159) epitaxially grown (undoped) $\text{InAs}_{0.61}\text{P}_{0.39}$ samples. The H_2 flow rates were varied in the range from 1780 cc/min for sample 153 to 515 cc/min for sample 159. The electron mobility is found to vary from $7800 \text{ cm}^2/\text{V-S}$ for sample 155 to $11300 \text{ cm}^2/\text{V-S}$ for sample 157 at 77°K , and the electron concentration varies slightly from $1.43 \times 10^{16} \text{ cm}^{-3}$ to $2.0 \times 10^{16} \text{ cm}^{-3}$. (2) Resistivity and Hall effect measurements yield the resistivity, Hall coefficient, electron concentration and electron mobility as a function of temperature (300°K to 3°K) for epitaxial samples 153 through 159 and bulk samples H-2, H-5 and H-6. (3) The activation energy of the donor states, the donor and acceptor densities and scattering mechanisms for electrons in $\text{InAs}_{1-x}\text{P}_x$ alloys were calculated and analyzed. (4) The alloy compositions were determined from the electron microprobe analysis. (5) The energy band gaps versus alloy compositions were deduced from the optical transmission data. (6) The absorption coefficients near the fundamental absorption edge were plotted as a function of wavelength for H-1, H-2, H-5, H-6, H-7 and W-16. (7) Scattering mechanisms and conduction process in the $\text{InAs}_{1-x}\text{P}_x$ alloy systems were analyzed over the temperature range from 300°K to 3°K .

TABLE OF CONTENTS

<u>Chapter</u>	Page
I. INTRODUCTION AND SUMMARY.	1
II. EXPERIMENTAL PROCEDURES	7
2.1 Material Preparation	7
2.1.1 Epitaxially grown $\text{InAs}_{1-x}\text{P}_x$ films	7
2.1.2 As-received bulk $\text{InAs}_{1-x}\text{P}_x$ samples.	10
2.1.3 Procedures for handling InAsP samples	11
2.2 Measurement Techniques	12
2.2.1 Resistivity and Hall effect measurements.	12
2.2.2 Optical transmission and reflectance measurements.	14
2.2.3 Electron microprobe analysis	16
III. EXPERIMENTAL RESULTS: EPITAXIAL $\text{InAs}_{0.61}\text{P}_{0.39}$ FILMS	30
3.1 Resistivity and Hall Coefficient	30
3.2 Electron Concentrations	32
3.3 Electron Mobilities	32
3.4 Energy Band Gap Versus Alloy Composition	33
3.5 Summary.	34
IV. EXPERIMENTAL RESULTS: BULK $\text{InAs}_{1-x}\text{P}_x$ SAMPLES (H-2, H-5, H-6, etc.)	42
4.1 Resistivity and Hall Coefficient	42
4.2 Electron Concentration and Mobilities	43
4.3 Optical Absorption Coefficient and Energy Band Gap	49
4.4 Summary	50
V. ANALYSIS OF RESULTS	57
5.1 Scattering Mechanisms	57

Chapter	Page
5.1.1 Ionized impurity scattering	57
5.1.2 Polar optical mode scattering	59
5.2 Donor and Acceptor Impurity Densities; Activation Energy of Donor States.	61
5.3 Impurity Hopping Conduction at Low Temperatures.	62
5.4 Energy Band Structure of InAsP	68
5.5 Summary.	70
VI. FUTURE PLANS.	72
VII. REFERENCES.	73

LIST OF FIGURES

Figure No.	Title	Page
1.	Schematic representation of the vapor-phase deposition apparatus for InAsP epitaxial films	21
2.	Dependence of epitaxial phosphorous concentration on concentration of PH_3 in the AsH_3 - PH_3 gas mixture.	22
3.	Experimental arrangement in block form for resistivity and Hall effect measurements	23
4.	Schematic diagram for optical transmission and reflectance measurements	25
5.	Optical path for a Perkin-Elmer (PE) model 98 prism monochromator.	26
6.	Wavelength versus drum turn of a PE-98 monochromator and the corresponding location of each InAsP sample deduced from absorption coefficient data	27
7.	(a) Schematic diagram of electron micorprobe analyser. (b) InAsP samples H_1 , H_2 , H_5 , H_6 , H_7 , Si and Ge were embedded into the copper filled <u>Diallyl Phthalate</u>	28
8.	Resistivity versus inverse absolute temperature for epitaxial samples 153, 154, 156, 157 and 159	36
9.	Hall coefficient versus inverse absolute temperature for epitaxial samples 153, 154, 156, 157 and 159 for $B = 5$ Kilogauss.	37
10.	Hall coefficient as a function of magnetic field for sample 155 at different temperatures.. . . .	38
11.	Hall coefficient as a function of magnetic field for sample 156 at different temperatures	39
12.	Electron concentration versus inverse absolute temperature for epitaxial samples 153, 154, 156, 157 and 159 deduced from Hall coefficient data at $B = 5$ Kilogauss and $\gamma = 1$	40
13.	Hall mobility versus inverse absolute temperature for epitaxial samples 153, 154, 156, 157 and 159, at $B = 5$ Kilogauss.	41

Figure No.	Title	Page
14.	Resistivity versus inverse absolute temperature for bulk samples H-2, H-5 and H-6.	45
15.	Hall coefficient versus inverse absolute temperature for bulk samples H-2, H-5 and H-6 at B = 5 Kilogauss . .	46
16.	Electron concentration versus inverse absolute temperature for H-2, H-5 and H-6 deduced from the Hall coefficient at B = 5 Kilogauss.	47
17.	Hall mobility versus inverse absolute temperature for H-2, H-5 and H-6 for B = 5 Kilogauss	48
18.	Transmission intensity versus wavelength for sample H-2 with two different thicknesses, Emission Spectrum of the Nernst globar source is also included	52
19.	Transmission intensity versus wavelength for sample H-6 with two different thicknesses.	53
20.	Absorption coefficient versus photon energy for samples H-1, H-2, H-5, H-6, H-7 and W-16	54
21.	Square of the absorption coefficient versus photon energy for samples H-1, H-2, H-5, H-6, H-7 and W-16. . .	55
22.	Energy Band gap versus alloy composition for both bulk and epitaxial $\text{InAs}_{1-x}\text{P}_x$ samples	56
23.	Resistivity versus absolute temperature for epitaxial samples 153, 154, 156, 157 and 159 for $3^\circ\text{K} < T < 25^\circ\text{K}$	66
24.	Resistivity versus absolute temperature for bulk samples H-2 and H-6 for $3^\circ\text{K} < T < 20^\circ\text{K}$	67
25.	Energy Band structure for InAs, InP and $\text{InAs}_{1-x}\text{P}_x$	69

LIST OF TABLES

Table No.	Title	Page
I.	Epitaxially grown $\text{InAs}_{1-x}\text{P}_x$ samples produced by vapor-phase techniques.	17
II.	Bulk $\text{InAs}_{1-x}\text{P}_x$ samples (H-series) produced by Czochralski techniques.	18
III.	Bulk $\text{InAs}_{1-x}\text{P}_x$ samples grown by the liquid encapsulation techniques (W-series)	19
IV.	Lap speed and polishing time for InAsP samples using IMACO multipol precision polishing machine	20
V.	Conductivity activation energies E_1 and E_3	35
VI.	Relative dielectric constant and effective mass ratio versus alloy compositions for some $\text{InAs}_{1-x}\text{P}_x$ alloys.	58
VII.	Calculated and experimental electron mobilities at 300°K for $\text{InAs}_{1-x}\text{P}_x$ samples.	64
VIII.	Donors and Acceptors Density, Activation Energy of Donor States for Epitaxial $\text{InAs}_{0.61}\text{P}_{0.39}$ Samples (300°K).	65

I. INTRODUCTION AND SUMMARY

This first semi-annual technical report covers the research activities from December 1973 to May 1974. The objectives of this project are to conduct the theoretical and experimental study of the basic electronic transport, recombination and scattering processes, impurities and defects, optical and structural properties in the bulk and the epitaxially grown $\text{InAs}_{1-x}\text{P}_x$ alloy systems and the GaSb epitaxial films for the 1-2 μm infrared photocathode and other IR device and system applications.

Specific material parameters to be determined from this study include (1) electron concentrations, electron mobilities and electron lifetimes as functions of temperatures (300°K to 3°K) and alloy compositions, (2) the impurity and defect energy levels and densities, (3) the optical absorption coefficients and the energy band gaps versus alloy compositions. In addition, detailed studies will be made on the effects of changing the growth conditions (such as hydrogen carrier gas flow-rates, epitaxial layer thickness and substrate orientations) on the electron densities and electron mobilities of the $\text{InAs}_{1-x}\text{P}_x$ epitaxial films. The goal of this particular study is to provide information for improving growth techniques so that high quality (i.e., lower carrier concentration and higher electron mobility) epitaxial films can be achieved.

The experimental tools employed in this reporting period include (1) resistivity and Hall effect measurements, (2) magnetoresistance measurements, (3) optical transmission measurements, and (4) the electron microprobe experiment. A new liquid helium refrigeration system has recently been installed in our laboratory for continuous monitoring of the temperatures of samples from 300°K to 3°K. Future experiments to be included in this research program are (1) photoluminescence experiment, (2) photoconductivity decay experiment, (3) reflectance measurement, and (4) thermally stimulated current measurements.

The major accomplishments in this period are summarized as follows:

(A) Epitaxially Grown $\text{InAs}_{1-x}\text{P}_x$ Films (Samples 147 through 159)

A study has been made on the epitaxial deposition of $\text{InAs}_{0.61}\text{P}_{0.39}$ on semi-insulating Cr-doped GaAs via the hydride system to determine whether the purity of the epitaxial layers could be improved by controlling the hydrogen carrier gas flow rate. Seven samples (153 to 159) have been prepared at a substrate temperature of 675°C, indium zone temperature of 900°C and the reaction zone at 950°C. In preparing these samples all parameters were held constant except that the H_2 carrier flow-rate which was divided evenly between the HCl and the $\text{AsH}_3 + \text{PH}_3$ mixture was varied. The total H_2 flow rates used were: sample-153 at 1780 cc/min, -154 at 1530 cc/min, -155 at 1280 cc/min, -156 at 910 cc/min, -157 at 730 cc/min, -158 at 570 cc/min, and -159 at 515 cc/min. The epitaxial layer thickness varies from 14.0 μm to 20.6 μm .

Resistivity, magnetoresistance and the Hall effect measurements were made for samples 153, 154, 155, 156, 157 and 159 as a function of temperature between 300°K and 3°K. Electron concentration and the Hall mobility were deduced from these measurements. The results of this study can be summarized as follows:

- (1) From the low temperature (below 77°K) resistivity versus the inverse temperature plot, it is found that the conductivity activation energy of the shallow-donor states is $E_1 = (2.61 \pm 0.6) \times 10^{-3}$ eV, and the thermal activation energy for impurity hopping conduction below 20°K is $E_3 = (4.54 \pm 2.0) \times 10^{-5}$ eV for all the samples studied. With the exception of samples 155 and 159, the resistivity is found to increase with decreasing H₂-carrier flow rate during the growth of the epitaxial layers. The electrical conductivity at low temperatures can be expressed by $\sigma(T) = C_1 e^{-E_1/kT} + C_3 e^{-E_3/kT}$, where C_1 and C_3 are independent of temperatures, E_1 and E_3 are the activation energies given above.
- (2) From the Hall mobility versus the inverse temperature plot, the electron mobility at 77°K is found to vary from 7800 cm²/V-S for sample-155 to 11300 cm²/V-S for sample 157. Except for samples 155 and 159, the electron mobility is found to increase with decreasing H₂ carrier flow-rate. The electron mobility in all samples is found to be
(1) limited by the polar optical mode phonon scattering for $T > 200^\circ\text{K}$, (2) dominated by the ionized impurity scattering between 100°K and 30°K.

- (3) The electron density at 77°K shows slight dependence on the H_2 flow-rate, varying between $1.43 \times 10^{16} \text{ cm}^{-3}$ and $2 \times 10^{16} \text{ cm}^{-3}$.
- (4) Impurity band conduction was observed for all samples at temperatures below 20°K, which can be attributed to the heavy compensation occurring (i.e., $N_A/N_D \gtrsim 0.1$) in these samples.
- (5) The magnetoresistance data shows that $\Delta\rho/\rho_0$ is largest for temperatures near 77°K, and diminishingly small for temperatures near 300°K and 4.2°K. This result is consistent with the scattering models described in (2) for these samples.
- (6) From the resistivity and the Hall coefficient data, it is concluded that normal band conduction process prevails for $T > 77^\circ\text{K}$, while impurity hopping conduction process dominates for $T < 20^\circ\text{K}$.
- (7) The alloy compositions of these films were determined by the electron microprobe method, the results are summarized in Tables II and III. The energy band gaps as functions of alloy compositions were deduced from the absorption coefficient data taken near the fundamental absorption edge.
- (8) The scattering mechanisms (mainly due to polar optical mode phonon and ionized impurity scatterings)) and the impurity hopping conduction process observed at low temperatures were discussed and analyzed for all the samples studied.
- (9) The donor and acceptor densities were calculated for samples 153 to 159 and the results are listed in Table VIII.

(B) Bulk InAs_{1-x}P_x Samples (H-1, H-2, H-5, H-6, H-7, W-16)

Resistivity and Hall effect measurements were performed for samples H-2, H-5 and H-6 between 300°K and 3°K. Electron densities and mobilities as a function of temperature were deduced from these measurements. Optical transmission and electron microprobe measurements were made for samples H-1, H-2, H-5, H-6, H-7 and W-16; the absorption coefficient and the energy band gap versus alloy compositions were deduced from these measurements. The results are summarized as follows:

- (1) The 77°K electron concentration was found to vary from $4.2 \times 10^{15} \text{ cm}^{-3}$ for H-6 to $1.8 \times 10^{16} \text{ cm}^{-3}$ for H-2, and the electron mobilities were found to vary from $11500 \text{ cm}^2/\text{V-S}$ for sample H-6 to $1.2 \times 10^5 \text{ cm}^2/\text{V-S}$ for sample H-5 at 77°K.
- (2) The electron mobilities as a function of temperature were deduced from conductivity and Hall coefficient data, and the results showed that the scattering mechanisms were dominant by polar optical mode phonon scattering for $T > 200^\circ\text{K}$ and by ionized impurity scattering for $T < 100^\circ\text{K}$. This is consistent with that observed in the epitaxial films.
- (3) Results of Hall coefficient data indicated that peak of the Hall coefficient shifts towards the higher temperature side as the impurity concentrations increased in these samples. Similar behavior has been observed in Ge and InSb by other investigators.⁽¹⁻²⁾
- (4) The densities of donors and acceptors in these samples were calculated and results are summarized in Table VIII.

- (5) Optical absorption coefficient from the transmission measurements indicates that these ternary alloy compounds are direct band gap materials with the energy band gap varied nearly linear with the alloy compositions over the entire alloy composition range.

II. EXPERIMENTAL PROCEDURES

2.1 Material Preparation

2.1.1 Epitaxially grown $\text{InAs}_{1-x}\text{P}_x$ Films (Samples 147 to 159)

Thirteen samples of vapor phase grown $\text{InAs}_{1-x}\text{P}_x$ epitaxial films⁽²⁾ deposited on semi-insulating (10^6 - 10^8 ohm-cm) Cr-doped GaAs substrates were prepared at the Air Force Cambridge Research Laboratories. These samples can be divided into two sets: InAsP-147 to InAsP-152 inclusive and InAsP-153 to InAsP-159 inclusive. In the first set the AsH_3/PH_3 ratio in the vapor phase was varied and with all other parameters held constant except for the deposition temperature which was 650°C for the first three samples and 675°C for the second three samples. The AsH_3/PH_3 ratio was adjusted to vary the As/P ratio in the epitaxial films. Analyses of P and As stoichiometry were done by the electron microprobe. Thus, the P-concentration (where the concentration of As + P = 100%) for each sample is: InAsP-147 = 3.4%P, InAsP-148 = 10%P, InAsP-149 = 20%P, InAsP-150 = 39.2%P, InAsP-151 = 62.4%P, and InAsP-152 = 77.4%P.

The second set of samples, InAsP-153 to InAsP-159, all had an AsH_3/PH_3 ratio equal to InAsP-150 and therefore should have a P concentration of 39.2%. For these samples all parameters were held constant except that the H_2 carrier flow-rate

which was divided evenly between the HCl and the $\text{AsH}_3 + \text{PH}_3$ mixture was varied. The total H_2 flow rates used were: InAsP-153 at 1780 cc/min., InAsP-154 at 1530 cc/min., InAsP-155 at 1280 cc/min., InAsP-156 at 910 cc/min., InAsP-157 at 730 cc/min., InAsP-158 at 570 cc/min., and InAsP-159 at 515 cc/min. The thickness of epitaxial layers varies between 14 μm to about 20 μm . A list of these epitaxial films along with some physical parameters are summarized in Table I. A schematic diagram of the vapor phase deposition apparatus is also shown in Fig. 1.

The reactant gases used to prepare these epitaxial samples were: anhydrous 99.995% HCl, 10% AsH_3 in H_2 , and 5% PH_3 in H_2 (impurity level for the PH_3 and AsH_3 mixtures was less than 1 ppm per component) obtained from Precision Gas Products, Inc. The H_2 carrier gas was standard grade purified by passage through a 1g-Pd diffuser. The In, obtained from the Indium Corp. of America had a reported purity of 99.999%. The substrates which were purchased from the Monsanto Co. were Cr doped semi-insulating GaAs ($\rho > 10^8$ ohm-cm) which were chemically polished on one side by Semiconductor Processing Co.

The H_2 carrier flow-rate for samples InAsP-147 to 152 inclusive was 2100 cc/min and this flow was divided almost evenly between the HCl and the $\text{AsH}_3\text{-PH}_3$ mixture. The HCl flow-rate for all samples was 7.7 cc/min. The AsH_3 and PH_3 flow-rate for samples InAsP-147-152 was varied from 0.7 cc/min-14 cc/min and 0.4 cc/min to 27 cc/min respectively to obtain

the desired $\text{InAs}_{1-x}\text{P}_x$ composition. The temperatures of the three heated zones of the deposition section are shown in Fig. 1.

The growth procedure used for these samples is described as follows: The deposition system through which H_2 always flows was brought to temperature. A freshly etched substrate was placed on the slotted sample holder at the end of the truebore rod. The truebore rod passes through a precision bore bearing equipped with a standard taper glass joint. The sample was inserted into the forechamber (the large 35 mm bore stopcock being closed) and the forechamber was flushed with H_2 for 15-30 min. Just prior to inserting the sample into the deposition section the $\text{AsH}_3 + \text{PH}_3 + \text{H}_2$ mixture flow is started. The H_2 carrier gas for the HCl which always flows is increased to run value. This prevents the $\text{AsH}_3 + \text{PH}_3$ mixture from reacting with the In. The 35 mm bore stopcock is opened and the truebore rod holding the sample is pushed through the stopcock inserting the substrate into the deposition zone. The HCl flow is started and deposition begins. When the run is completed the sample is drawn back into the forechamber, the stopcock closed and the gas flow stopped. The forechamber is flushed with H_2 , and the sample removed.

Substrate preparation - As received from Semiconductor Processing Co. the substrates were chemically polished on one side and lapped on the other. The substrate was degreased in boiling trichloroethylene, and etched for 30-45 minutes in a 5:1:1 solution of Caro's acid ($\text{H}_2\text{SO}_4:\text{H}_2\text{O}_2:\text{H}_2\text{O}$), in an inclined,

rotating, Teflon beaker. The substrate was removed from the Caro's acid, rinsed in deionized H_2O and methanol and then etched for 2 minutes in a 0.5% Br_2 methanol solution. The substrate was then rinsed in methanol and blown dry with filtered He.

It is also worth noting that the P/As + P ratio in the deposited layer is not equal to the $PH_3/AsH_3 + PH_3$ ratio used in the vapor phase. Fig. 2 shows this relationship for the hydride system used; the result was determined by electron-microprobe analysis and flowmeter readings for deposits of the $InAs_{1-x}P_x$ on InAs.* This same figure has been used to determine the approximate flows to grow samples of InAsP-147 through 159.

2.1.2 Bulk $InAs_{1-x}P_x$ samples (H-series and W-series samples)

Twelve specimens of bulk $InAs_{1-x}P_x$ ingots with different alloy compositions were received from Naval Research Laboratories, Pasadena Branch Office. The physical parameters and alloy compositions of these samples were summarized in Tables II and III. These samples were originally grown by Bell & Howell, Inc. Two different techniques had been used to prepare these crystals. The H-series samples were grown by the sealed Czochralski technique. The W-series specimens were grown by the liquid encapsulation technique.⁽³⁾ Most of these samples are polycrystalline crystals with large grain size. It was also noticed that as the doping densities (e.g., Sn, Te and Se) were increased the grain size tended to decrease. In addition, nearly all of the ingots were pulled from nonstoichiometric melts of $In_{1-y}(As_{1-x}P_x)_y$ where $y = 0.40-0.45$ ($y = 0.50$ corresponds to a stoichiometric melt).

*Fig. 2 was provided by Dr. J. Kennedy of AFCRL.

2.1.3 Procedures for handling InAsP samples

An InAsP compound semiconductor is a very soft and fragile material which is easily subjected to surface damage. Therefore, a crucial portion of any experiment using this material is strongly dependent upon sample preparation involving cutting and polishing.

Sample cutting was accomplished by using an AB Isomet low speed saw. The saw has been developed for precision, low deformation cutting of materials such as GaP, InP, CdS, InAs and other compound semiconductors.

Samples approximately 1 cm x 2mm x 1 mm were cut by using a 3" diameter by 0.010" thick diamond wafering blade.

Sample polishing was done by using the IMACO Multipol Precision polishing machine. This is a variation of the Droper System whereby the sample is swept back and forth across one side of the lap, while rotating about its own center, as the lap rotates underneath. This greatly improved the flatness of the sample, and reduced the tendency of Comet trails.

Several interchangeable glass plates, some with polishing cloths attached, can be fixed to the stainless steel lap place, providing quick and easy changeability of polishing conditions. In order to maintain maximum flatness a precision polishing jig with conditioning ring attached was used. The conditioning ring being used to maintain the flatness of the lap where otherwise high zones on the lap would develop because of the lightly loaded specimen.

A four-step polishing procedure has been used starting with a coarse grit silicon carbide powder; this is shown in Table IV.

The resulting InAsP samples show optical flatness and are readily used for optical transmission, reflectance, electron-microprobe analysis, and carrier lifetime measurements.

2.2 Measurement Techniques

2.2.1 Resistivity and Hall-effect measurements

The experimental technique employed to measure the resistivity and Hall voltage was the standard Van der Pauw ⁽⁴⁾ method except in the case of sample H-5 which was measured by conventional methods. ⁽⁵⁾ The experimental setup shown in Fig. 3 was used for these measurements. The sample leads were connected to a switching panel which allowed for switching of the current and voltage leads. In the case of resistivity measurements the eight voltage readings needed were read directly from the Keithley 640 for each temperature, then averaged by computer. For Hall effect measurements the magnetic field was swept from 0 to 5000 gauss. The magnetic field was monitored by a Bell 620 Gaussmeter, the output of which was fed into the y-axis of an EA1 1130 x-y plotter. Again a total of eight voltage measurements were needed in the Van der Pauw method due to current reversal, magnetic field reversal, and interchange of the current and voltage leads. The output of the Keithley 640 was the source for the x-axis of the plotter. Values from the eight resulting curves at each temperature were taken from the plots and again fed into the computer for calculation of the Hall coefficient and carrier concentration.

Sample cooling was achieved with a Model LT-3-110 Liquid Helium Transfer Heli-Tran Refrigerator. The temperature was continuously variable from about 3°K to 300°K. However the liquid helium consumption rate was in the range of 0.7 liquid liters per hour so liquid nitrogen was used for the temperature range of 77.3°K to 300°K because of cost considerations. The temperature was normally stable to within $\pm 0.1^\circ\text{K}$ and was measured with a chromel vs. gold 0.07 at .90 iron thermocouple. Thermocouple readings were made with a Honeywell Model 2783 six-dial potentiometer.

Sample preparation consisted of scribing and cleaving the epitaxial samples to obtain a rectangular piece usually on the order of one half centimeter per side. The bulk samples H-2 and H-6 were cut to obtain thin wafers, then a rectangular piece was cut from the center of each wafer with size comparable to the epitaxial samples (153-159). These pieces were then mechanically polished to assure a uniform thickness. All sample dimensions were then measured by a microscope adapted with a micrometer eyepiece. By placing the epitaxial samples on edge the epitaxial layer was easily recognized and measured. Measurements of the epitaxial layer were taken on each side of the sample then averaged.

Cleaning of the samples was accomplished by ten minute ultrasonic baths in trichloroethylene, acetone, then methanol. Immediately after the cleaning process, copper leads were soldered to each edge of the samples, halfway between the corners. Pure indium was used for the contacts and each contact was tested

for ohmicity. These contacts were characteristically 0.02 cm in width decreasing slightly with practice. After the contacts were made the sample was placed on a copper heat sink in the cryostat using Cry-Con grease as an adhesive and to assure good thermal contact.

From resistivity and Hall effect measurements, the carrier concentration, electron mobility, energy level of donors and acceptors, and density of donors and acceptors are determined.

2.2.2 Optical transmission and reflectance measurements

These two measurements are designed for determining the absorption coefficients versus wavelength for the InAsP alloy systems as well as energy band gaps versus alloy compositions. The experimental setup for this is shown in Fig. 4. The optical path for a Perkin-Elmer model 98 prism monochromator is shown in Fig. 5.

Samples were prepared in two different thicknesses through optical polishing techniques. A Multipol precision polishing machine was used to obtain identical optically flat surfaces on different samples thicknesses. Aluminum oxide grinding and polishing powders of 12 μ , 7.5 μ , 1 μ , 0.3 μ and 0.05 μ were used. Surfaces were checked and compared using 40x power optics through a microscope. Thicknesses were determined and flatness was measured using a Granit-chek with a 0.0001" Fowler gauge.

The optical transmission was measured for each sample using Perkin-Elmer-98 spectrophotometer equipment. The basic units included a Nernst globar light source, a NaCl prism monochromator, a 70x power microscope attachment for beam condensing

to handle small sample sizes, and a thermocouple detector with KBr windows and appropriate amplification circuits. This equipment was used to obtain optical transmission measured in 10^{-3} volts versus wavelength for each sample. One of the most important characteristics of this measurement system was that the absorption edge of the majority of these $\text{InAs}_{1-x}\text{P}_x$ samples fall within the most sensitive region of the system. This region was between 1μ - 2μ , and was not affected by water vapor in the optical path.

The absorption coefficients were determined from the measured optical transmission. This was done by noting that the transmission, T , is related to α the absorption coefficient by the equation[†]

$$T = (1-R)^2 e^{-\alpha d} \quad (2-1)$$

where d = thickness of the sample

R = reflection coefficient

Using samples of two different thicknesses, α can be calculated from equation (2-4).

$$T_1 = (1-R)^2 e^{-\alpha d_1} \quad (2-2)$$

$$T_2 = (1-R)^2 e^{-\alpha d_2} \quad (2-3)$$

Thus,

$$\alpha = \frac{2.3 \log(T_1/T_2)}{(d_2 - d_1)} \quad (2-4)$$

In this report, only the results from the transmission measurements were included, the results of reflectance measurements will be presented in the next interim-technical report.

The wavelength versus drum turn for a PE-98 monochromator is displayed in Fig. 6, along with the location of each InAsP sample deduced from absorption coefficient data.

2.2.3 Electron microprobe analysis

The schematic diagram of the electron microprobe which was used successfully to determine the As to P ratio of samples H1, H2, H5, H6, and H7 is shown in Fig. 7. The electron probe x-ray microanalyzer contains an electron optical column which generates a very small diameter beam of high energy electrons. The electron beam is focused on the surface of the specimen, which is viewed by an optical microscope. As a result of the electron bombardment, the specimen gives off characteristic x-rays corresponding to the elements present. The x-rays are analyzed by diffracting them with a crystal and measuring them with an appropriately positioned detector. The diffracting crystal and detector comprise the heart of the x-ray spectrometer. The output of the detector, consisting of electrical pulses of varying amplitude, is analyzed by means of several electronic signal processing equipment for both qualitative and quantitative measurements. The concentration of a specific element is determined by comparing the relative intensities generated by the element in the unknown and a standard. In order to obtain maximum accuracy, this ratio is then corrected for absorption and fluorescence of the emitted x-rays.

The samples to be analyzed were all embedded in diallyl phthalate, having a copper filler (see Fig. 7). A standard metallurgical thermosetting molding cycle, using an Adolph Buehler

Simplimet press, was used to embed the semiconductive samples in the mount. This facilitated polishing, conductive mounting in the electron microprobe and insured all processing steps for each sample to be identical.

A Cameca MS-64 electron microprobe, made by Acton Laboratories, Inc., was used to determine the As to P ratio. The analysis was based on background corrected x-ray intensities of the sample compared to standards of As, In, and InP. The relative x-ray intensities for an electron-beam having a 1μ diameter, 20 keV potential, and an x-ray takeoff angle of 18.0° were obtained for each sample. This information was entered into a computer program for quantitative microprobe analysis, MAGIC III, which performs all the necessary corrections needed to give the mean chemical composition in atomic percent. The results of this microprobe analysis is given in Table II.

Table I Epitaxially Grown $\text{InAs}_{1-x}\text{P}_x$ Samples
Produced by Vapor-Phase Techniques

<u>Sample No.</u>	<u>% of InP[†]</u>	<u>Deposition Temperature</u>	<u>H₂ Flowrate</u>
147	3.4%	650°C	2250 cc/min
148	10%	650°C	2250 cc/min
149	20%	650°C	2250 cc/min
150	39.2%	675°C	2250 cc/min
151	62.4%	675°C	2250 cc/min
152	77.4%	675°C	2250 cc/min
153	39.2%	650°C	1780 cc/min
154	39.2%	650°C	1530 cc/min
155	39.2%	650°C	1280 cc/min
156	39.2%	650°C	910 cc/min
157	39.2%	650°C	730 cc/min
158	39.2%	650°C	570 cc/min
159	39.2%	650°C	515 cc/min

[†] (1) The percentage of InP was calculated taking into account only the group V constituents. These percentages were determined by the Electron Microprobe Analysis.

(2) Epitaxial layer thickness about 20~30 μm .

(3) Substrates are semi-insulating Cr-doped GaAs with $\rho \sim 10^8 \Omega\text{-cm}$.

(4) As + P = 100%

Table II Bulk InAs_{1-x}P_x Ingots
Produced by Czochralski Technique

Ingot No.	Dopant	a_o (Å)	x	Atomic Percentage of InAsP as Determined by Electron Microprobe Analysis		
				In:	As:	P:
H1	--	5.975	0.43	49.15%	28.74%	22.11%
H5	--	5.940	0.75 0.63	49.99%	12.46%	37.57%
H6	--	5.9003	0.77	49.73%	11.70%	38.57%
H7	--	5.8872	0.89	50.31	5.37%	44.32%
H20	Te	5.898	0.85	-	-	-
H2	--	5.944	0.41	49.13%	29.86%	21.01%
H23	Se	5.8962	0.86	-	-	-

Table III Bulk InAs_{1-x}P_x Crystals*
Grown by the Liquid
Encapsulation Technique

<u>Ingot No.</u>	<u>Dopant</u>	<u>Mol. Fraction InP (x)</u>
W11	Se	0.845
W13	Se	0.130
W16	None	1.00
W23	Sn	0.845
W20	Te	0.845

*All data were taken at room temperature. The values of composition, x, were derived from x-ray powder photographs assuming Vegard's Law is valid.

Table IV Lap Speed and Polishing Time for InAsP Samples
Using IMACO Multipol Precision Polishing Machine

Lap	Abrasive Solution	Lab Speed	Polishing Time	Load
1st lap	1000 Grit, SiC	50 rpm	Till flat	w/weight
2nd lap	1 μm Al_2O_3	75 rpm	8 min.	w/weight
3rd lap	0.3 μ Al_2O_3	75 rpm	10 min.	w/weight
4th lap	0.05 μ Al_2O_3	75 rpm	25 min.	no weight

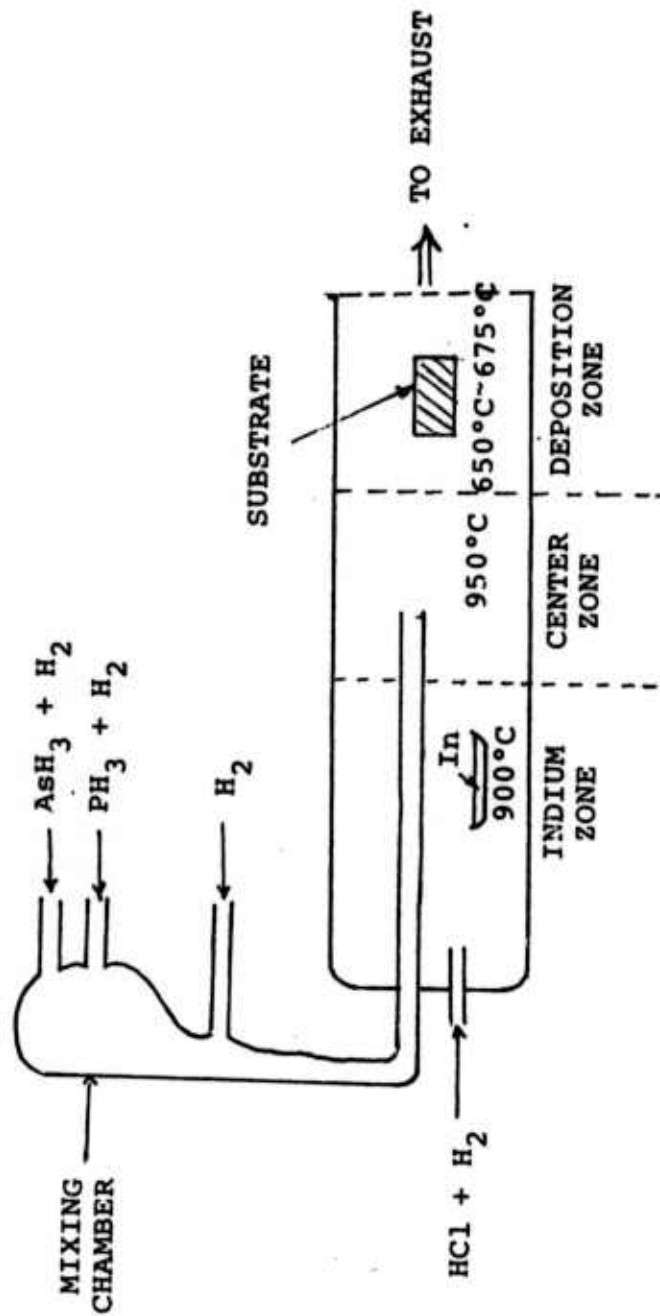


Fig. 1 Schematic representation of the vapor phase-deposition apparatus for $\text{InAs}_{1-x}\text{P}$ epitaxial films.

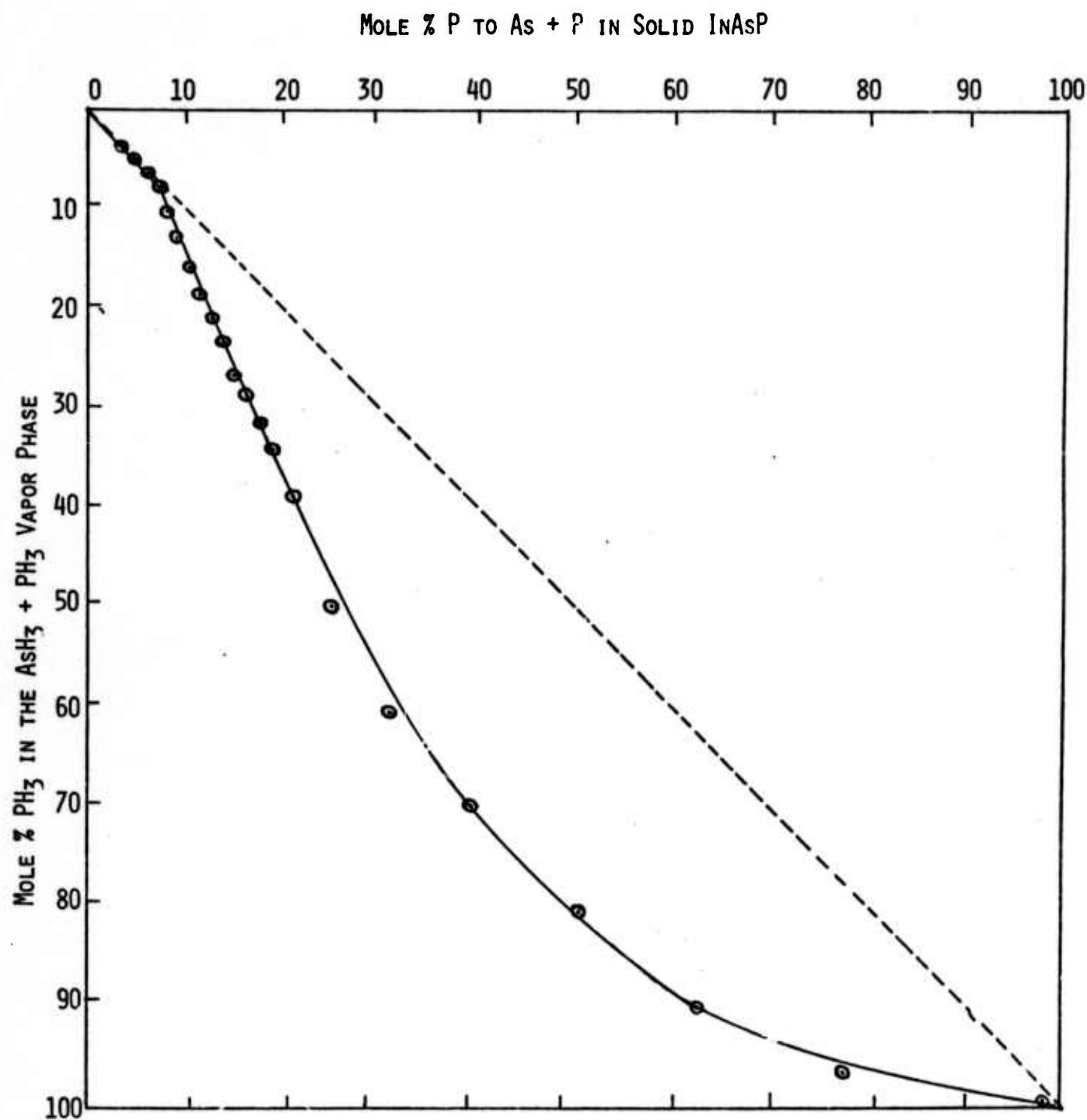


Fig. 2 Dependence of epitaxial phosphorous concentration of PH_3 in the AsH_3 - PH_3 gas mixture.

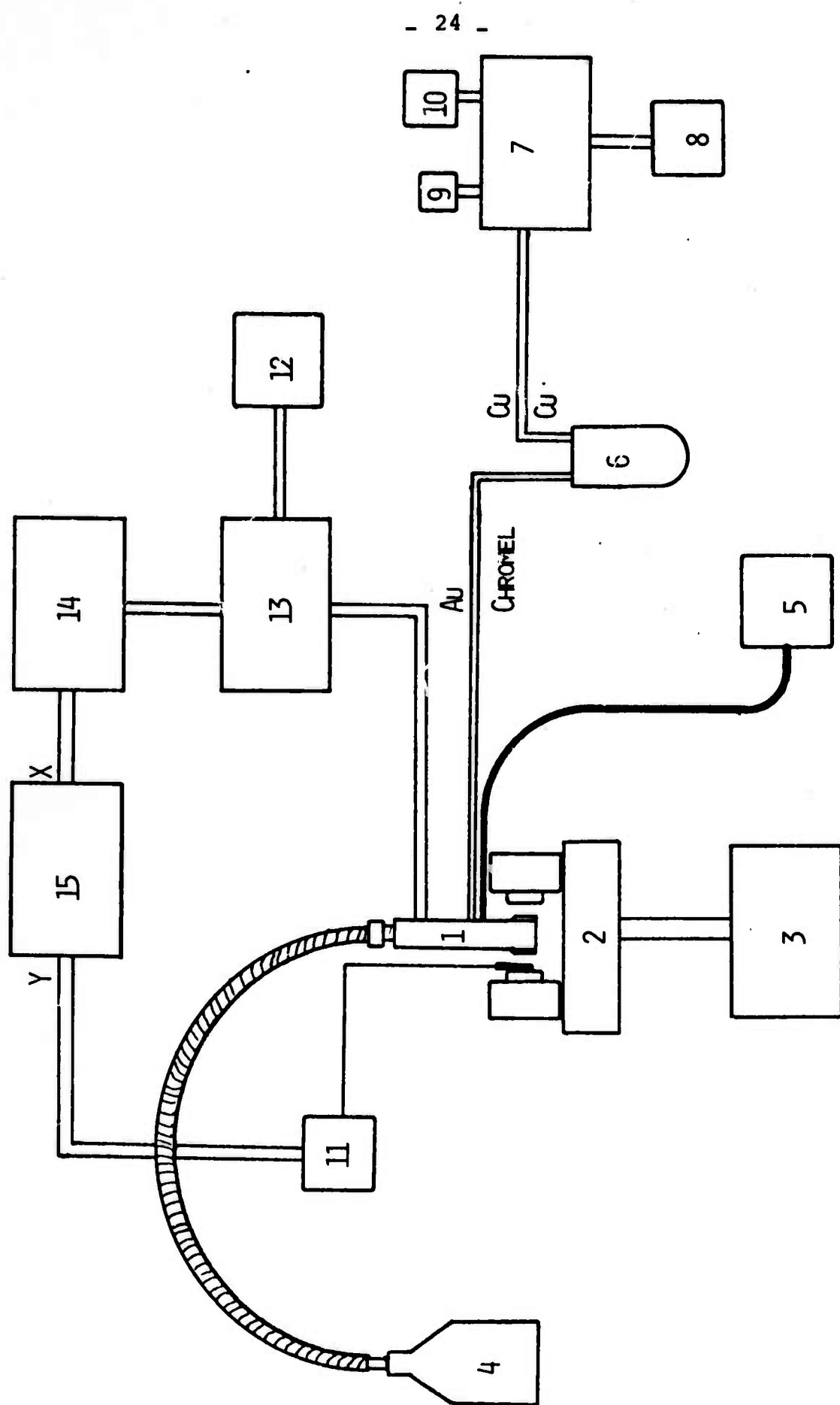


FIG. 3

Fig. 3 Experimental Setup for Measuring Resistivity and Hall Effect

- 1) Heli-Tran Model LT-3-110 cold tip
- 2) Varian V-3703 electromagnet
- 3) Varian sweep power supply
- 4) Liquid helium dewar
- 5) Vacuum Pump
- 6) Deionized ice bath
- 7) Honeywell Model 2783 potentiometer
- 8) Hewlett-Packard Model 425A DC Micro Volt-Ammeter
- 9) Standard cell
- 10) Six volt current source
- 11) Bell Model 620 gaussmeter
- 12) Keithley 261 Picoampere Source
- 13) Control panel
- 14) Keithley 640 Electrometer
- 15) EAI 1130 Variplotter

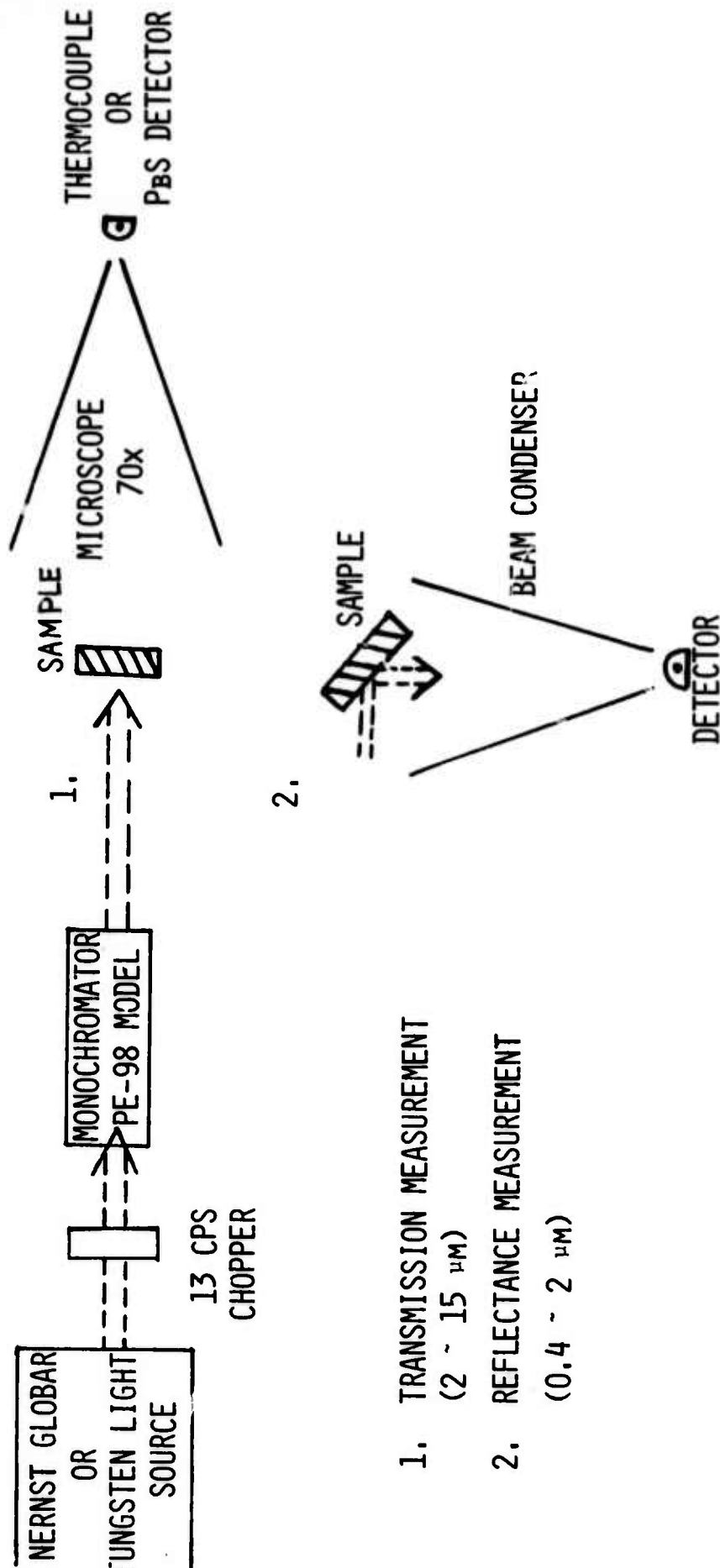


FIG. 4 SCHEMATIC DIAGRAM FOR OPTICAL TRANSMISSION AND REFLECTANCE MEASUREMENTS

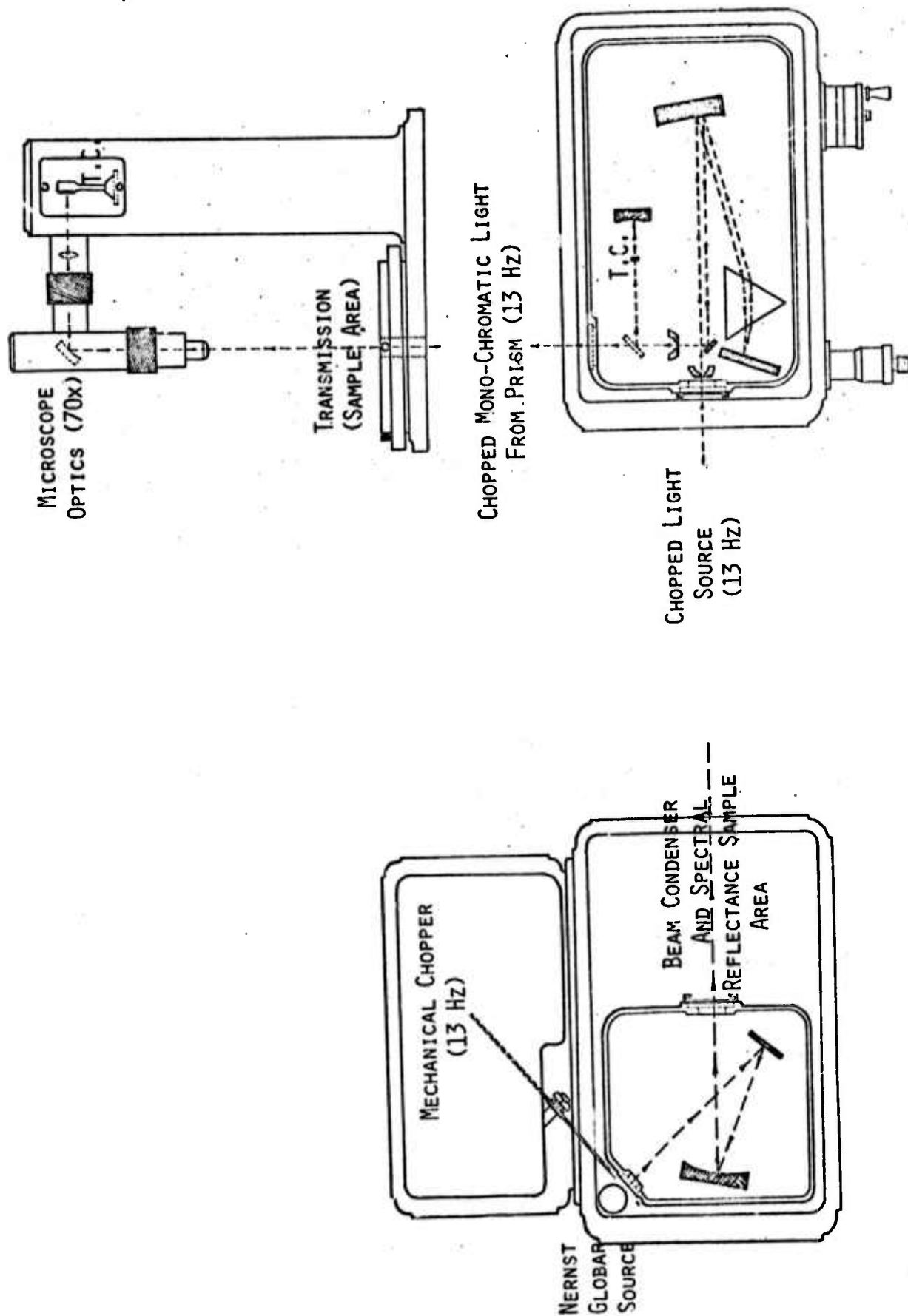


FIG. 5 OPTICAL PATH OF MODEL 98 SINGLE BEAM INFRARED SPECTROPHOTOMETER WITH INTERCHANGEABLE PRISMS AND ATTACHMENTS.

DRUM TURNS VERSUS WAVELENGTH FOR NaCl PRISM
(PERKIN-ELMER MODEL 98)

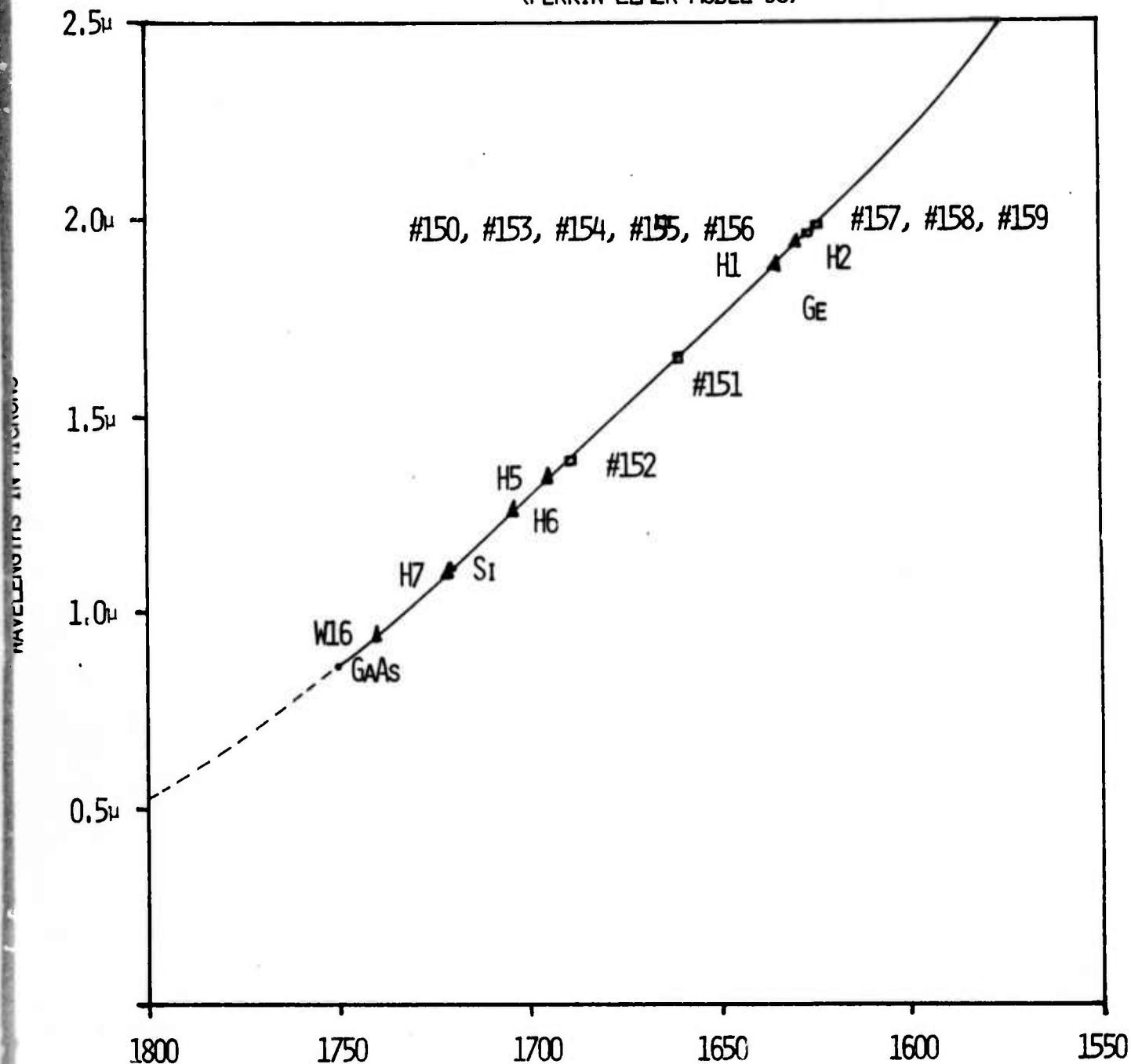
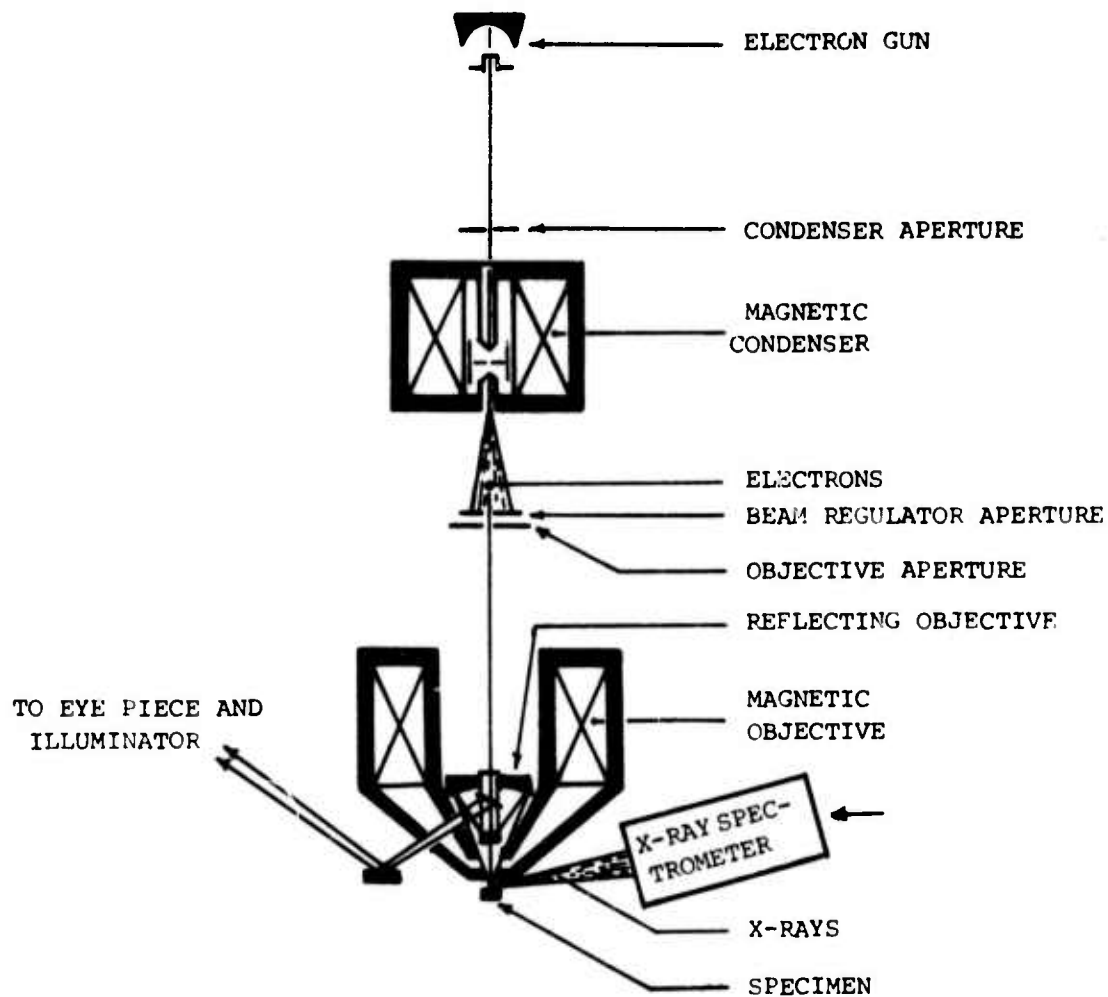
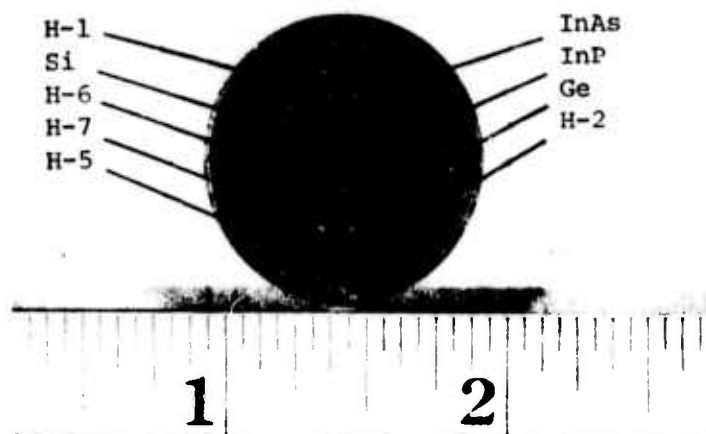


FIG. 6 WAVELENGTH VERSUS DRUM TURN OF PE-98 MONOCHROMATOR AND THE CORRESPONDING LOCATION OF EACH INAsP SAMPLE DEDUCED FROM ABSORPTION COEFFICIENT DATA.



(a)



(b)

Fig. 7 (a) Schematic diagram of electron microprobe analyser.
 (b) InAsP samples H₁, H₂, H₅, H₆, H₇, Si and Ge were embedded into the copper filled Diallyl Phthalate.

III. EXPERIMENTAL RESULTS: EPITAXIAL $\text{InAs}_{0.61}\text{P}_{0.39}$ Films

3.1 Electrical Resistivity and Hall Coefficient

Resistivity and Hall effect measurements have been made for epitaxially grown $\text{InAs}_{0.61}\text{P}_{0.39}$ samples -153, -154, -155, -156, -157 and -159 between 3°K and 300°K. Fig. 8 shows the resistivity versus inverse absolute temperature for these samples, respectively. The results show that resistivity first decreases exponentially with decreasing temperature for temperatures between 300°K and 77°K which is expected from the normal band conduction process and reaches a minimum around 77°K; the resistivity then increases exponentially with decreasing temperatures for temperatures between 77°K and 20°K with an activation energy of $E_1 = (2.61 \pm 0.6) \times 10^{-3}$ eV; below 20°K, the resistivity varies linearly with temperature (see Fig. 23), as the impurity hopping conduction dominates the conduction process. The thermal activation energy for hopping conduction is found to be $E_3 = (4.54 \pm 2.0) \times 10^{-5}$ eV for these samples. Thus, the low temperature conductivity curve (i.e., $T < 77^\circ\text{K}$) can be represented approximately by

$$\sigma(T) = c_1 e^{-E_1/kT} + c_3 e^{-E_3/kT} \quad (3-1)$$

where c_1 and c_3 are constants (independent of temperature).

Values of E_1 and E_3 for both epitaxial and bulk InAsP samples are summarized in Table V. The temperature dependence of the conductivity for the above epitaxial films is similar to the behavior of Ge specimens that were studied earlier by Fritzsche.⁽¹⁾ The results of this indicate that these epitaxial films are highly compensated with donors and acceptors. This is indeed the case as to be discussed later. The present results also show that except samples -159 and -155 the resistivity decrease with decreasing hydrogen carrier gas flow-rates (as it varies from 1780 cc/min for 153 to 515 cc/min for 159). Fig. 9 shows the Hall coefficient versus the inverse absolute temperature for samples 153, 154, 156, 157 and 159, for magnetic flux density $B = 5$ Kilogauss. The results show that the Hall coefficient first increases with decreasing temperature for $50^\circ\text{K} < T < 300^\circ\text{K}$, and reaches a maximum value for $T \sim 50^\circ\text{K}$ and then approaches a constant value for $T < 20^\circ\text{K}$. From the above results, it is found that the maximum value of the Hall coefficient occurs at 58°K for -153, 53°K for -154, 50°K for -156, 49°K for -157, 56°K for -155 and 53°K for -159. It is further noted that the peak value of the Hall coefficient for each sample shifts towards higher temperature side as the H_2 flow-rate is increased (with the exception of samples -155 and -159). This implies that the impurity densities are indeed increased with the increasing H_2 flow-rate during the growth of the epitaxial layer via

hydride system, although the change of carrier density is not appreciable in the present case.

The magnetic field dependence of the Hall coefficient for samples 155 and 156 are shown in Fig. 10 and Fig. 11, respectively for different temperatures. The results show that the Hall coefficient in both samples depends very weakly on the magnetic field for temperatures above 200°K and below 20°K. However, for $20^{\circ}\text{K} < T < 80^{\circ}\text{K}$, the Hall coefficient depends rather strongly on the magnetic field, implying that ionized impurity scattering process prevailed over this temperature range ($\gamma = 1.93$ for ionized impurity scattering).

3.2 Electron Concentrations

The electron concentration can be calculated from the Hall coefficient data using the relation

$$n = \frac{\gamma}{eR_H} \quad (3-2)$$

where γ is the scattering factor varying between 1 and 2, depending on the types of scattering processes involved. For simplicity, we assume $\gamma = 1$ and calculate the values of n from (3-2). The result is shown in Fig. 12. The 77°K electron concentration is found to vary between $1.45 \times 10^{16} \text{cm}^{-3}$ and $1.9 \times 10^{16} \text{cm}^{-3}$ for five epitaxial samples described above.

3.3 Electron Mobility

The Hall mobility was obtained from the resistivity and the Hall coefficient data shown in Fig. 8 and Fig. 9 using the relation

$$\mu_H = \sigma R_H$$

(3-3)

The result is illustrated in Fig. 13 for samples 153 through 159. It is interesting to note that the Hall mobility (or electron mobility) is independent of H_2 flow-rates for temperatures above 200°K implying that the polar optical mode phonon scattering dominates in this temperature range. The ionized impurity scattering, however, prevails for temperatures around 77°K. The 77°K electron mobility varies from 7800 $\text{cm}^2/\text{V-S}$ for sample -155 to 11300 $\text{cm}^2/\text{V-S}$ for sample -157. With the exception of samples -155 and -159, the electron mobility does increase with decreasing H_2 flow-rates, although the change in electron mobility is not so significant.

The magnetoresistance study on the above samples revealed that these specimens showed very small magnetoresistance effect near room temperatures and at very low temperatures (i.e. below 20°K) and shows maximum magnetoresistance effect near 77°K. Details of this study will be included in the next interim technical report.

3.4 Energy Band Gap and the Alloy Composition

The energy band gap versus the alloy composition for thirteen epitaxially grown $\text{InAs}_{1-x}\text{P}_x$ alloy films was determined from the optical transmission and electron microprobe measurements. The energy band gaps were deduced from the sharp transition edge observed near the fundamental absorption edge by optical transmission

experiment. The results of this was displayed in Fig. 22 along with the results for bulk samples. Since only one thickness was available for each epitaxial film it was impossible for us to determine the absorption coefficient versus photon wavelength from this single transmission experiment.

3.5 Summary

Study of the epitaxial deposition of $\text{InAs}_{0.61}\text{P}_{0.39}$ on semi-insulating Cr-doped GaAs via the hydride system has been made to determine whether the purity of the epitaxial layers could be improved by the proper control of the growth conditions. Seven samples have been prepared at a substrate temperature of 675°C and with H_2 carrier flow-rate varying from 1780 cc/min to 515 cc/min. The epitaxial thickness varies from 14 μm to about 20 μm . Results of resistivity and Hall effect measurements on these samples between 300°K and 3°K show a change of electron concentration from 1.45×10^{16} to $2 \times 10^{16} \text{ cm}^{-3}$ and of electron mobility from 7800 to 11300 $\text{cm}^2/\text{V-S}$ at 77°K . Since the variation in electron concentration in these samples is not appreciable and the samples studied are limited, further study is needed before any conclusion can be reached.

TABLE V.
Conductivity Activation Energies* E_1 and E_3 for
Bulk and Epitaxial $\text{InAs}_{1-x}\text{P}_x$ Samples

Samples	Thickness	$E_1 (\times 10^{-3}) \text{ eV}$	$E_3 (\times 10^{-5}) \text{ eV}$
153	17.46 μm	3.22	4.88
154	14.45 μm	3.08	2.07
155	20.60 μm	2.75	5.54
156	16.63 μm	2.40	7.53
157	14.01 μm	2.42	2.85
159	15.47 μm	1.80	4.34
H-2	.03433 cm	2.77	5.15
H-5	-	4.60	-
H-6	.03945 cm	6.29	12.74

$$*\sigma(T) = c_1 e^{-E_1/kT} + c_3 e^{-E_3/kT}$$

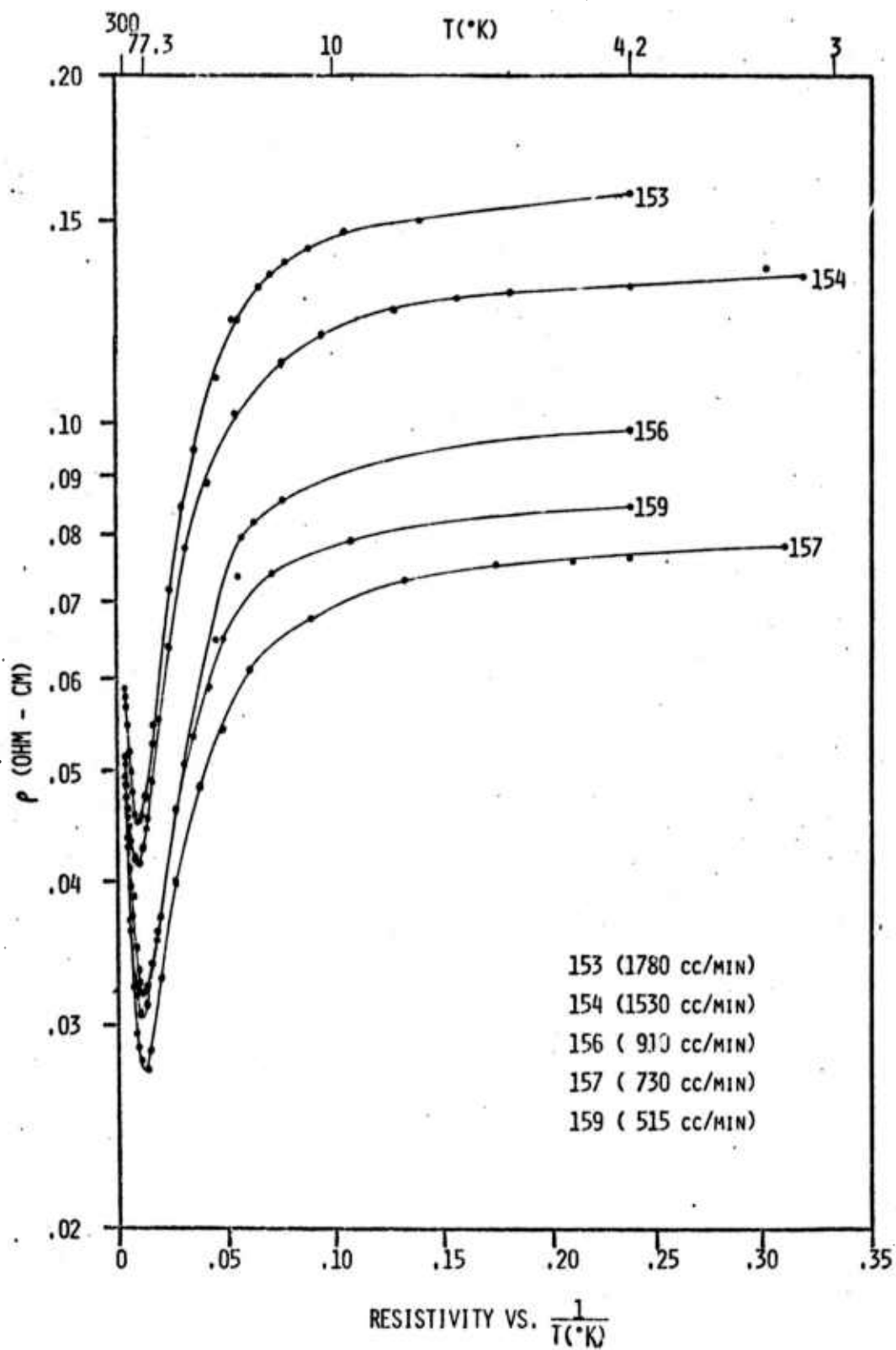


Fig. 8 Resistivity versus inverse absolute temperature for epitaxial samples 153, 154, 156, 157 and 159.

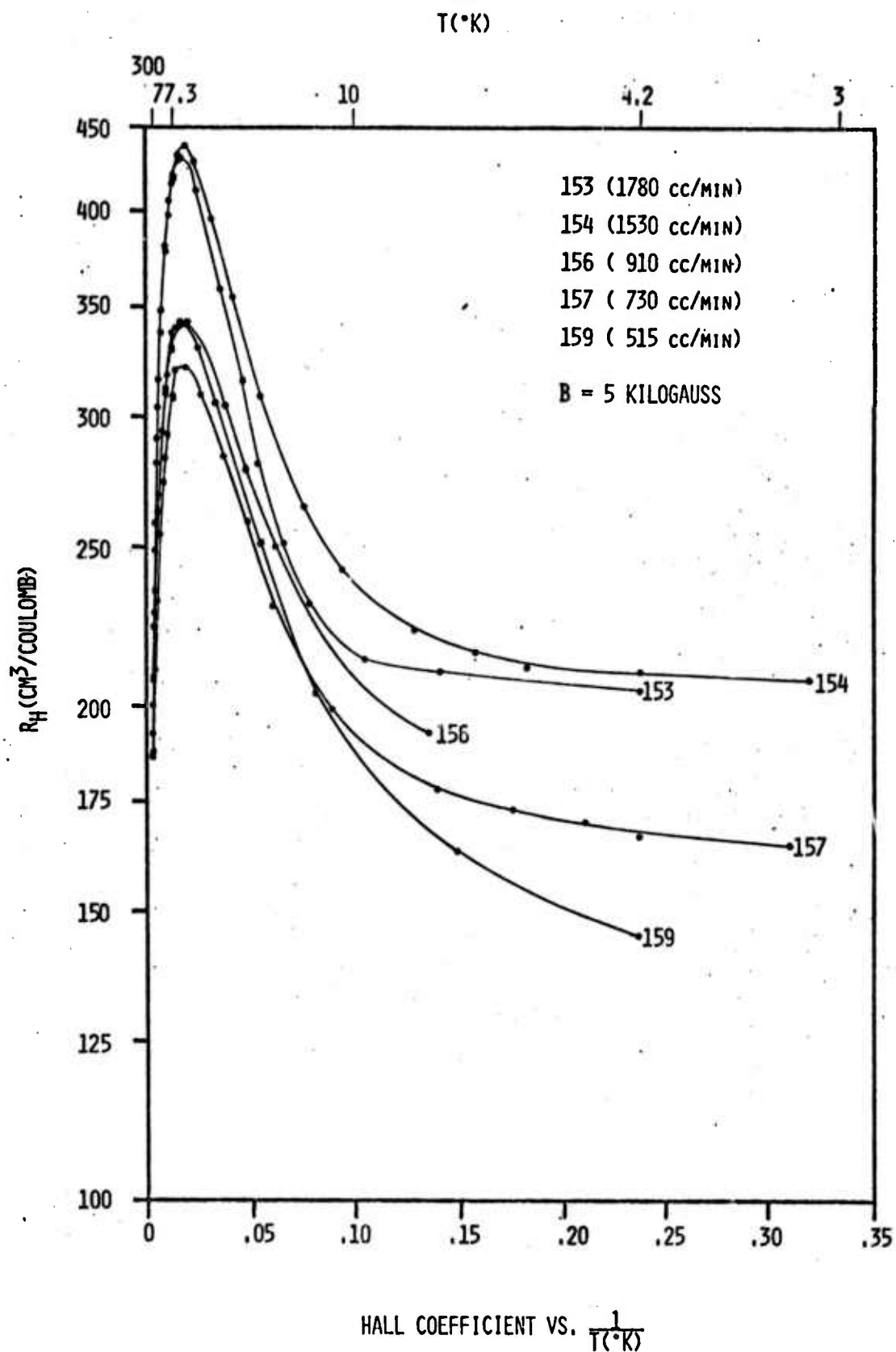


Fig. 9 Hall coefficient versus inverse absolute temperature for epitaxial samples 153, 154, 156, 157 and 159 for $B = 5$ Kilogauss.

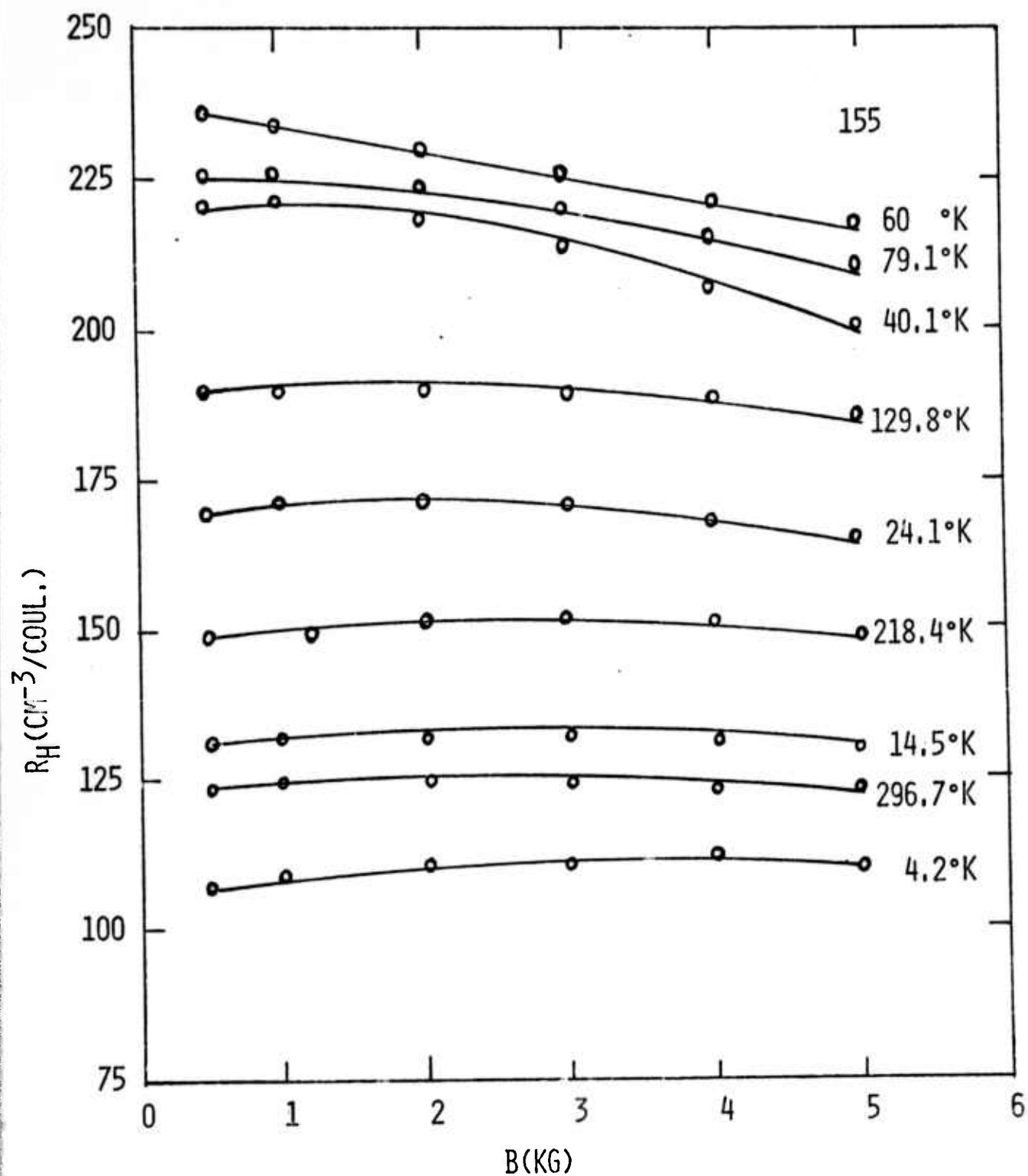


FIG. 10 HALL COEFFICIENT AS A FUNCTION OF MAGNETIC FIELD FOR SAMPLE 155 AT DIFFERENT TEMPERATURES.

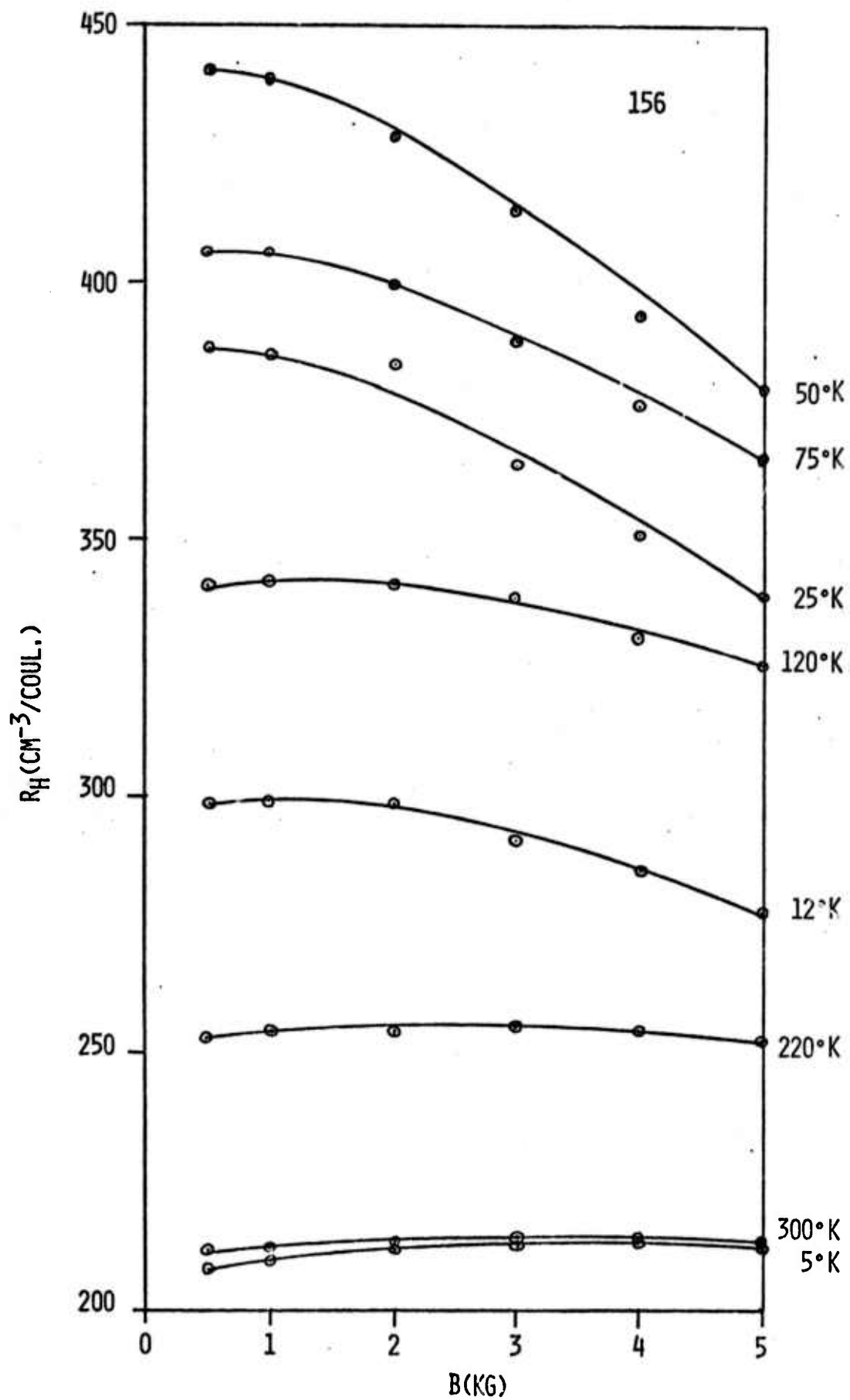


Fig. 11 Hall Coefficient as a function of magnetic field for sample 156 at different temperatures.

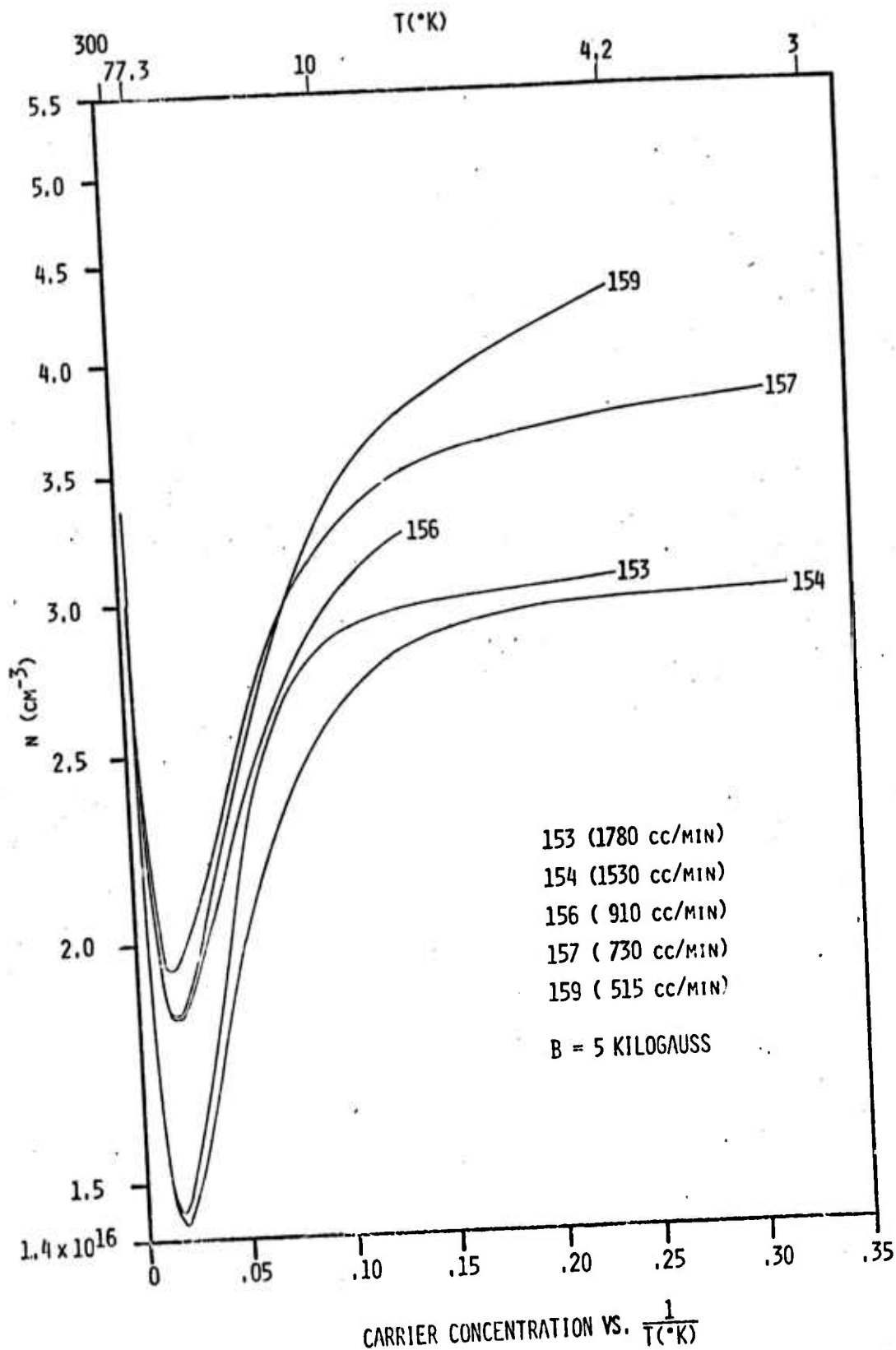


Fig. 12 Electron concentration versus inverse absolute temperature for epitaxial samples 153, 154, 156, 157 and 159 deduced from Hall coefficient data at $B = 5$ Kilogauss and $\gamma = 1$.

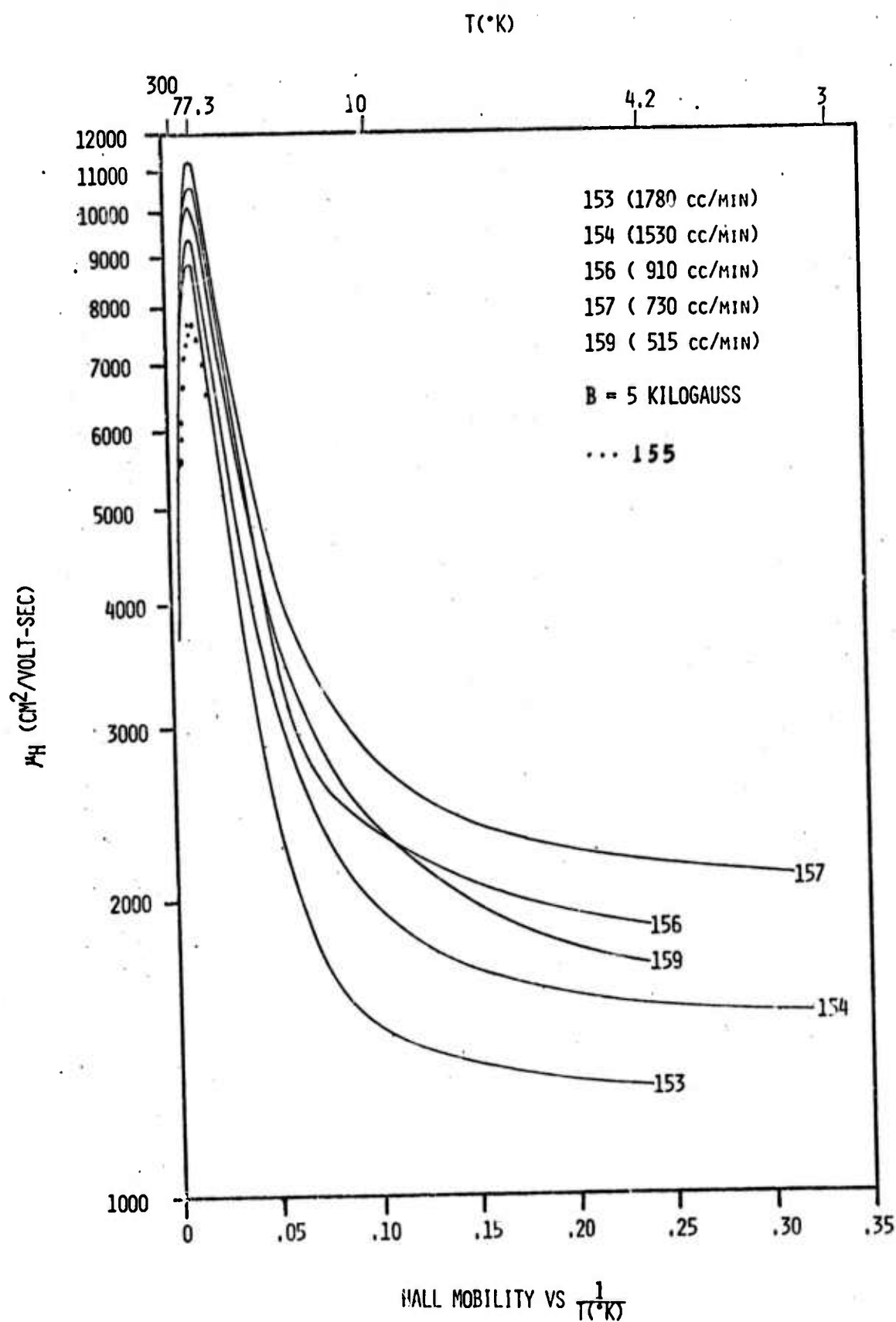


Fig. 13 Hall mobility versus inverse absolute temperature for epitaxial samples 153, 154, 156, 157 and 159, at B = 5 Kilogauss.

IV. EXPERIMENTAL RESULTS: BULK $\text{InAs}_{1-x}\text{P}_x$ Samples (H-2, H-5, H-6, etc.)

4.1 Hall Coefficient and Electrical Resistivity

Results of the resistivity and Hall effect measurements on H-2, H-5 and H-6 were shown in Fig. 14 and Fig. 15, respectively, for temperatures between 300°K and 3°K. These samples were undoped and grown by Czochralski technique. Sample H-2 has 41% P and 59% As; H-5 has 63% P and 37% As, and H-6 has 77% P and 23% As.

The general behavior of the temperature dependence of the resistivity and the Hall coefficient for these bulk samples was similar to that observed for the epitaxial samples -153 through -159 discussed in the previous chapter. However, the impurity concentrations and resistivity in these samples change more drastically from sample to sample than that observed in the epitaxial films.

From Fig. 14 it is noted that the resistivity first decreases exponentially with decreasing temperatures and reaches a minimum value at 77°K, it then increases exponentially with temperature with an activation energy of $E_1 = (5.45 \pm 0.85) \times 10^{-3}$ eV for samples H-5 and H-6 and $E_1 = (2.77) \times 10^{-3}$ eV for H-2 for $10^\circ\text{K} < T < 77^\circ\text{K}$ (for values of E_1 and E_3 see Table V). The resistivity

varies linearly with temperature for $T < 10^\circ\text{K}$ (see Fig. 24), indicating that the impurity hopping conduction process prevails at very low temperatures.

The Hall coefficient versus the inverse temperature was displayed in Fig. 15. The results show that peak of the Hall coefficient shifts towards the higher temperature side for samples with higher impurity concentrations; this behavior was also observed earlier in germanium samples by Fritzsche.⁽¹⁾ The Hall coefficient becomes fairly constant at very low temperatures when the conduction mechanism is dominant by the impurity hopping conduction process.

4.2 Electron Concentrations and Electron Mobilities

The electron concentration versus the inverse temperature for H-2, H-5 and H-6 was shown in Fig. 16. The results show that room temperature electron concentration varies from $5.2 \times 10^{15} \text{ cm}^{-3}$ for H-6 to $3.4 \times 10^{16} \text{ cm}^{-3}$ for H-2. The Hall mobility was calculated by using Eq. (3-3) and the data shown in Fig. 14 and 15; the result is shown in Fig. 17. Note that the electron mobility for H-2 and H-6 is comparable to that of the epitaxial samples 153-159. However, the electron mobility for sample H-5 is anomalously high and may need further investigation. Since this is the first sample (H-5) we measured, the reliability of the data was questionable. Further study for sample H-5 will be conducted during the third quarter of this contract and the results will be presented

in the next technical report.

From Fig. 17 it is noted that the polar optical mode phonon scattering dominates the scattering mechanism for $T > 200^{\circ}\text{K}$ and the ionized impurity scattering prevails for temperatures between 77°K and 20°K . The impurity hopping conduction process dominated for temperatures below 10°K . This is consistent with that observed in the epitaxial samples discussed in the previous chapter.

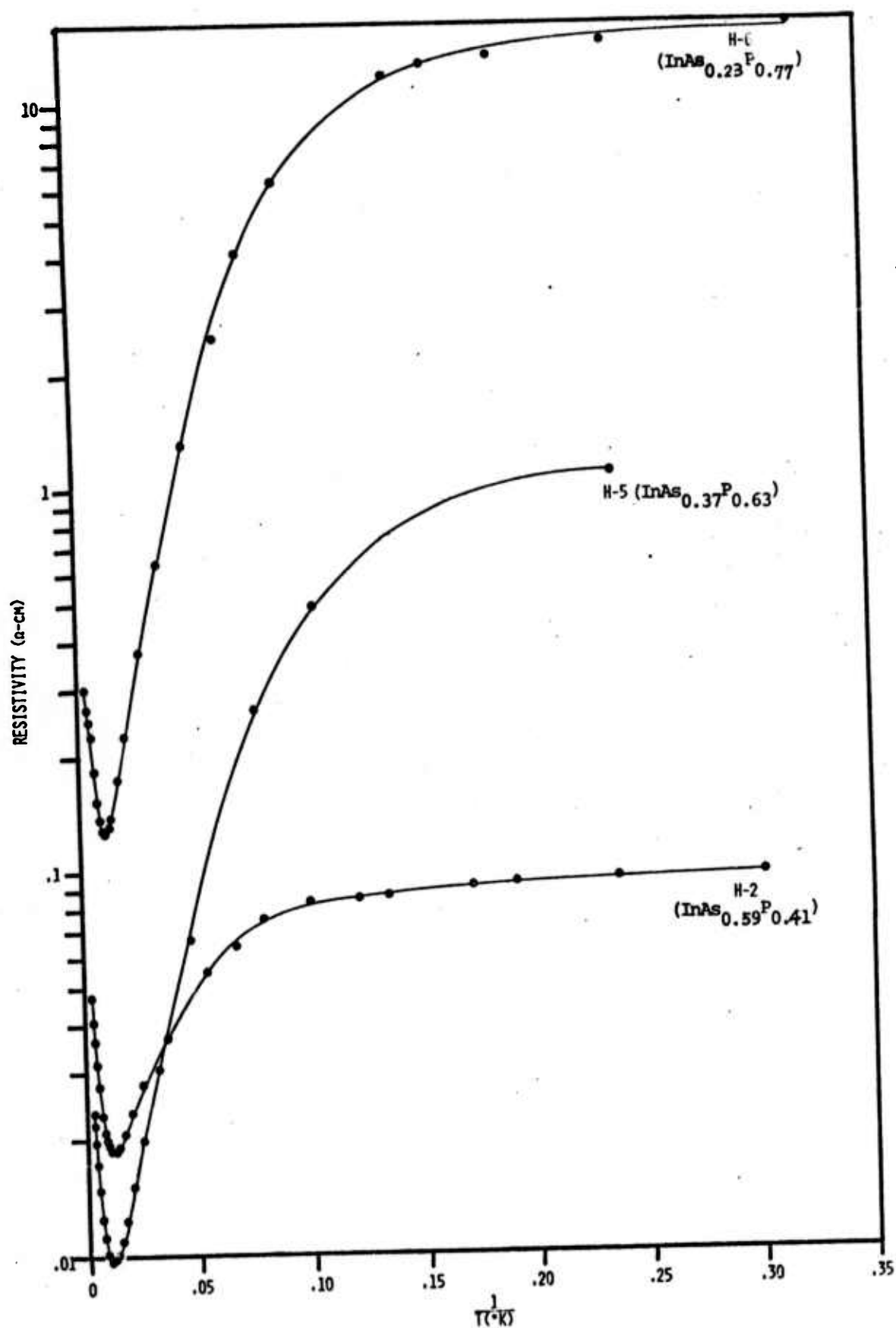


Fig. 14 Resistivity versus inverse absolute temperature for bulk samples H-2, H-5 and H-6.

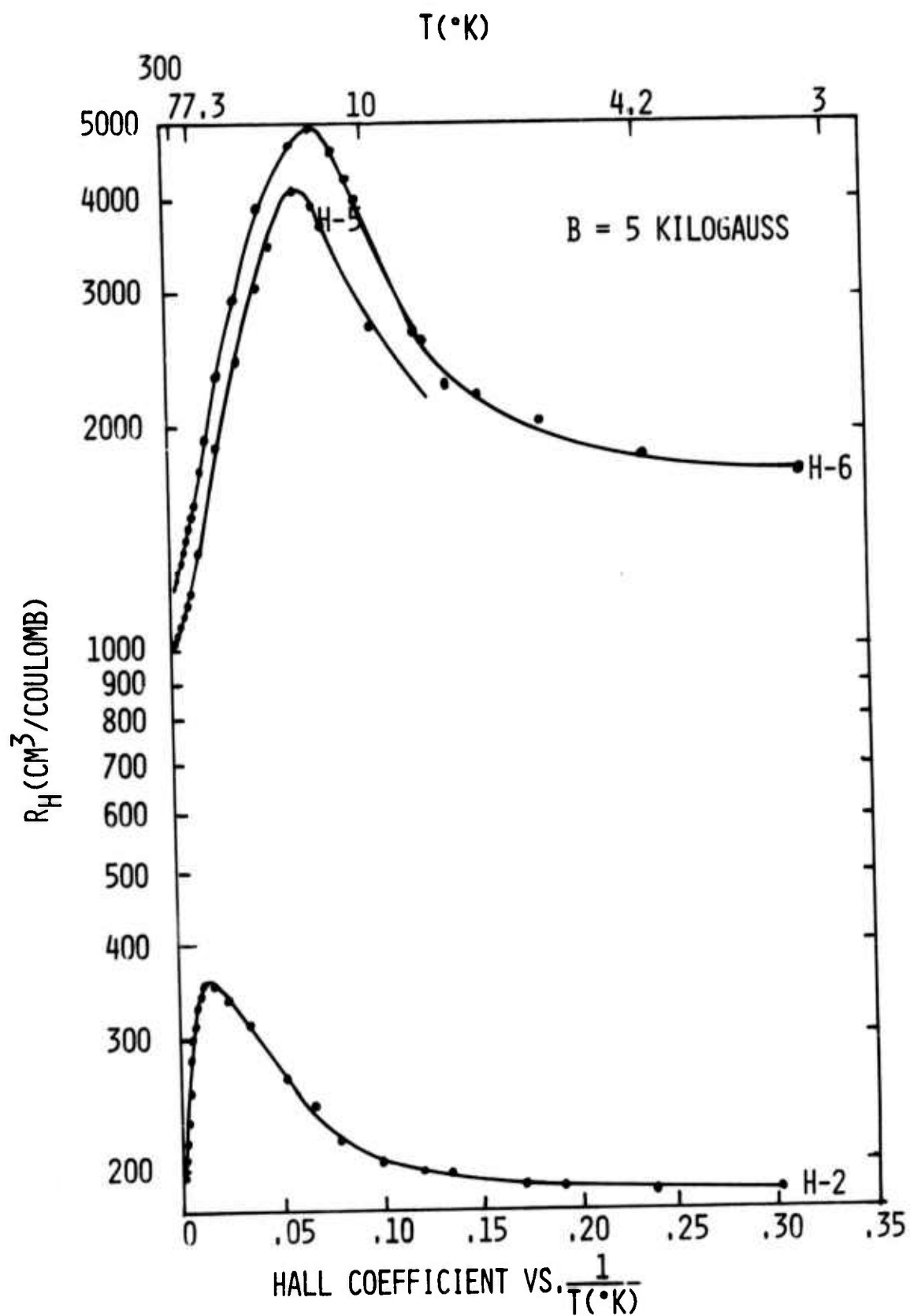


FIG. 15 HALL COEFFICIENT VERSUS INVERSE ABSOLUTE TEMPERATURE FOR BULK SAMPLES H-2, H-5 AND H-6 AT $B = 5$ KILOGAUSS.

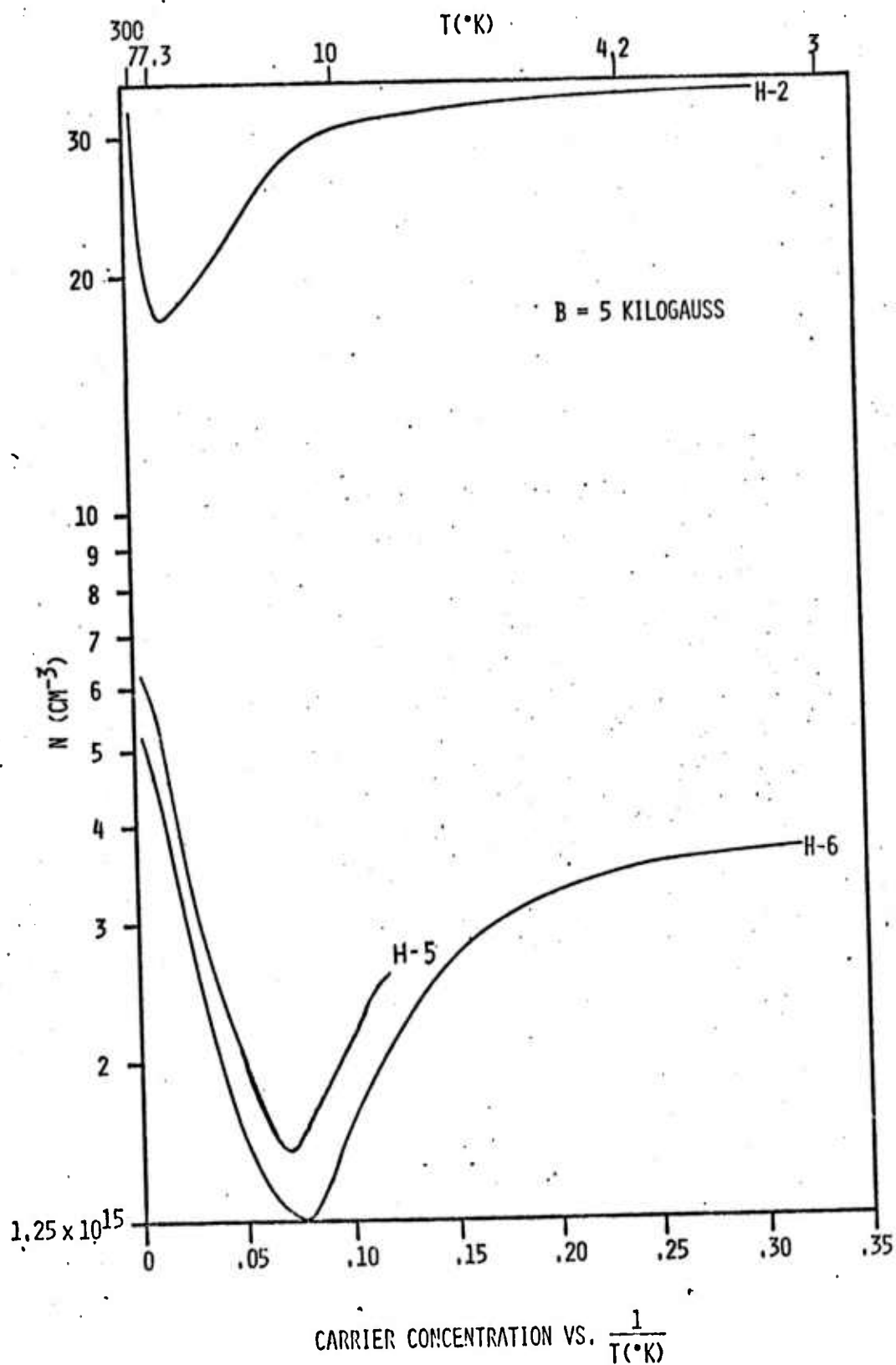


Fig. 16 Electron concentration versus inverse absolute temperature for H-2, H-5 and H-6 deduced from the Hall coefficient at $B = 5$ Kilogauss.

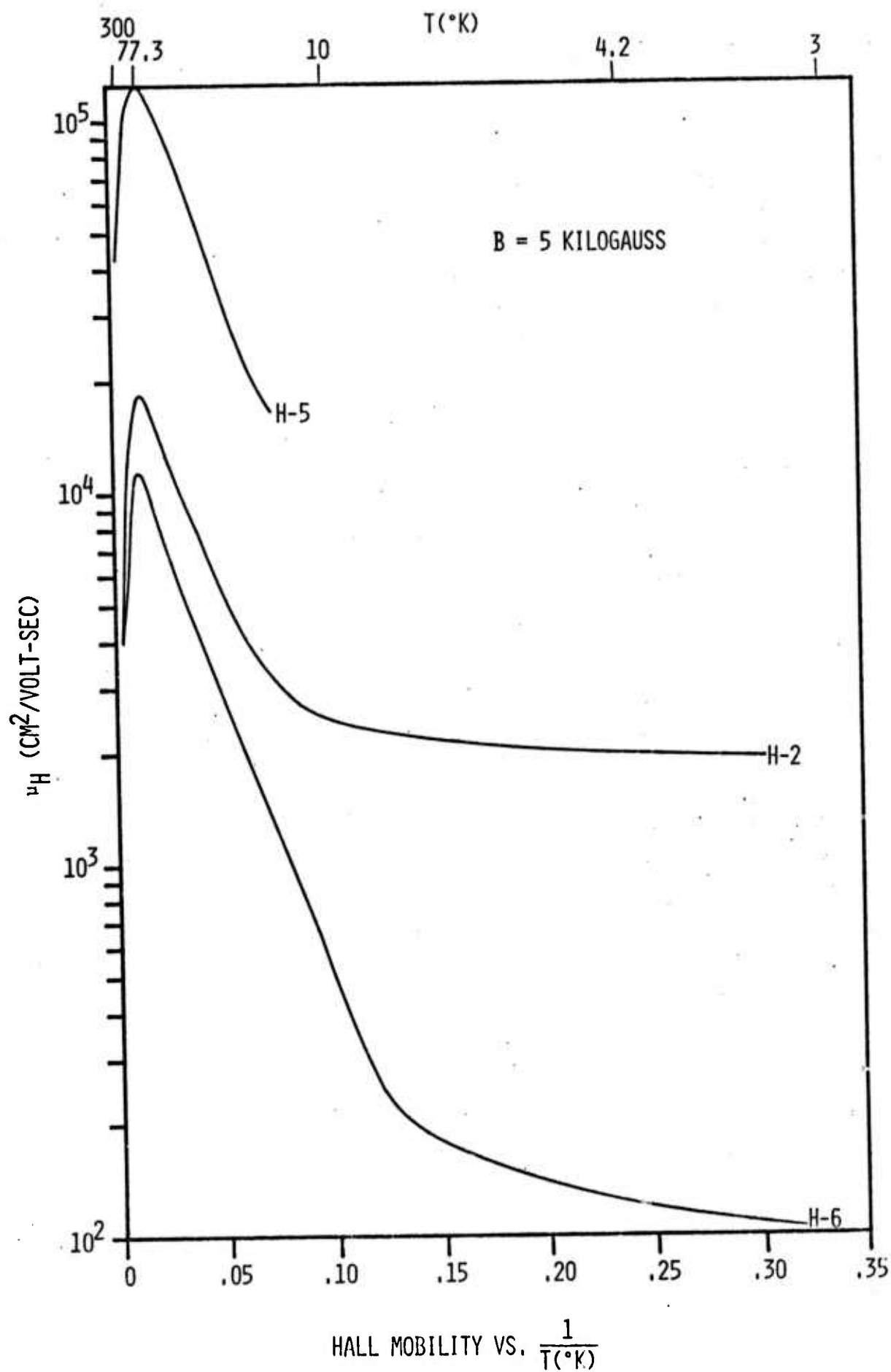


FIG. 17 HALL MOBILITY VERSUS INVERSE ABSOLUTE TEMPERATURE

4.3 Optical Absorption Coefficient

Optical transmission measurements have been performed for samples H-1, H-2, H-5, H-6, H-7 and W-16 from 1 μm to 15 μm wavelength range. Fig. 18 and Fig. 19 showed the transmission intensity versus wavelength for H-2 and H-6, respectively. The absorption coefficient was calculated by using Eqs. (2-2), (2-3) and (2-4). The absorption coefficient versus photon energy for six bulk samples was displayed in Fig. 20. These are the absorption data near the fundamental absorption edge of each alloy composition. The energy band gap for each alloy composition can be estimated from this graph. To deduce the energy band gap for each alloy composition and to assess the energy band structure of these ternary alloy compounds, the square of the absorption coefficient was plotted as a function of photon energy and the result was shown in Fig. 21. From Fig. 21 it is noted that the following relation holds true at the higher photon energy part of each curve

$$\alpha^2 \sim (h\nu - E_g) \quad (4-1)$$

where α is the absorption coefficient, $h\nu$ is the photon energy and E_g is the energy band gap of the material.

The linear dependence of α^2 on the photon energy $h\nu$ shown in Fig. 21 indicates that all these $\text{InAs}_{1-x}\text{P}_x$ samples are direct band gap semiconductors. The variation in the alloy composition, x , from InAs to InP only alters the energy band gap between the conduction band minimum and the valence band maximum at $\Gamma = 0$ of the Brillouin zone.

By extrapolation of the linear portion of α^2 versus $h\nu$ at the higher-energy part of the curve to the intercept of $h\nu$ axis yields the energy band gap E_g for sample with different alloy composition.

Fig. 22 shows the energy band gap versus alloy compositions for both bulk and epitaxial $\text{InAs}_{1-x}\text{P}_x$ samples that were studied during this research period. The alloy compositions were obtained from the electron microprobe experiment.

4.4 Summary

Resistivity and Hall effect measurements have been performed for samples H-2, H-5 and H-6 between 300°K and 3°K. Electron concentrations and electron mobilities as a function of temperature were deduced from these measurements. The results show that the electron density varies from $5.2 \times 10^{15} \text{ cm}^{-3}$ for H-6 to $3.3 \times 10^{16} \text{ cm}^{-3}$ for H-2 at 300°K, and electron mobility varies from $4000 \text{ cm}^2/\text{V-S}$ for H-2 and H-6 to $3.3 \times 10^4 \text{ cm}^2/\text{V-S}$ for H-5. From the temperature dependence of electron mobility it is concluded that the polar optical mode phonon scattering dominates for $T < 200^\circ\text{K}$. The impurity hopping conduction process was observed at very low temperature ($T < 10^\circ\text{K}$). The above results are in good agreement with the results obtained for the epitaxially grown InAsP samples discussed in the previous chapter.

The absorption coefficient versus photon wavelength near the fundamental absorption edge were deduced from the optical transmission measurements for samples H-1, H-2, H-5, H-6, H-7 and W-16. From the square of the

absorption coefficient versus photon energy plot the energy band gap was deduced for each sample and the direct band gap structure was confirmed for these ternary compounds. The energy band gap as a function of alloy composition was obtained over the entire composition range for $\text{InAs}_{1-x}\text{P}_x$ samples. The band gap was found to vary linearly with the alloy compositions for the $\text{InAs}_{1-x}\text{P}_x$ alloy system.

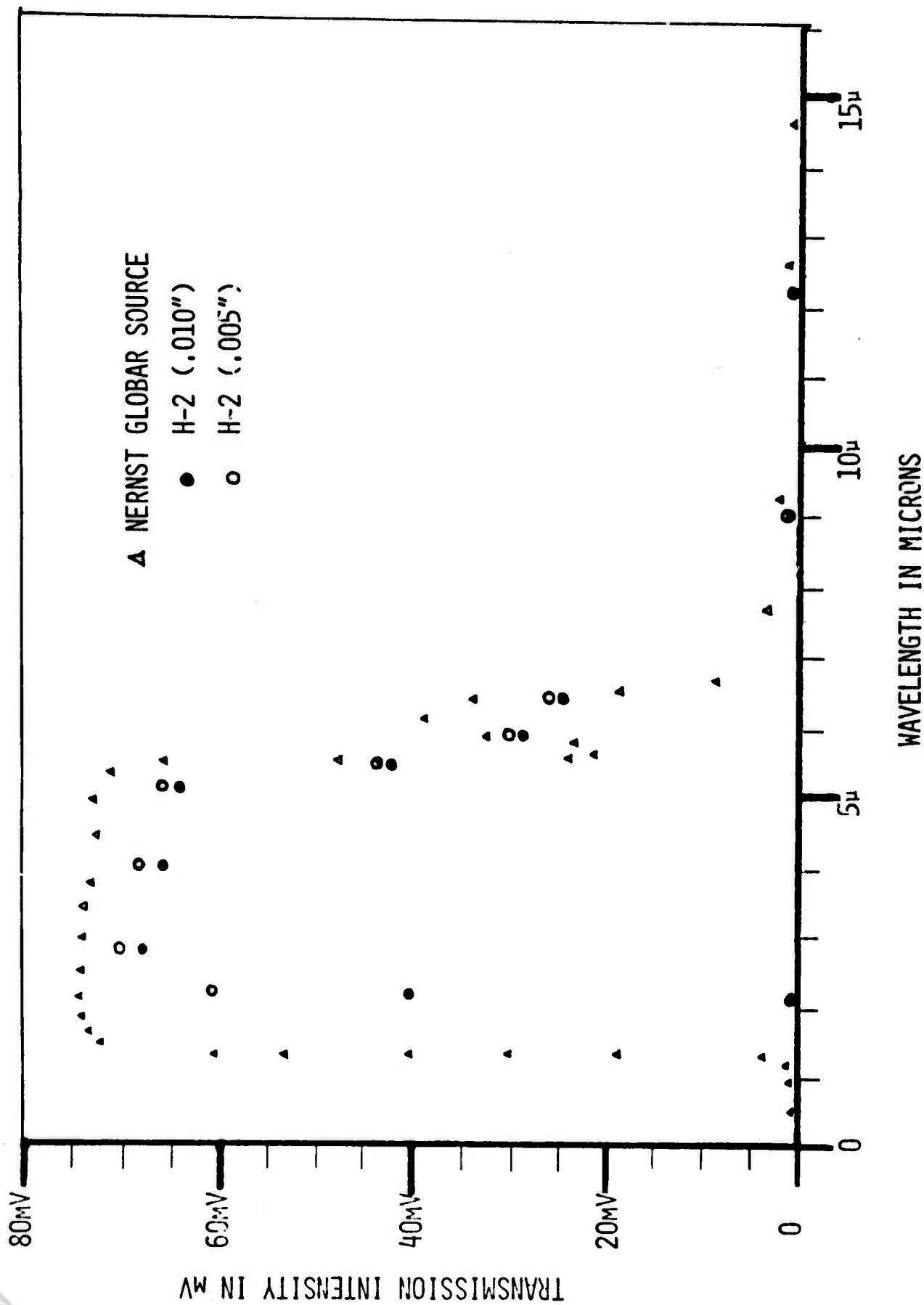


Fig. 18 Transmission intensity versus wavelength for sample H-2 with two different thicknesses, Emission Spectrum of the Nernst global source is also included.

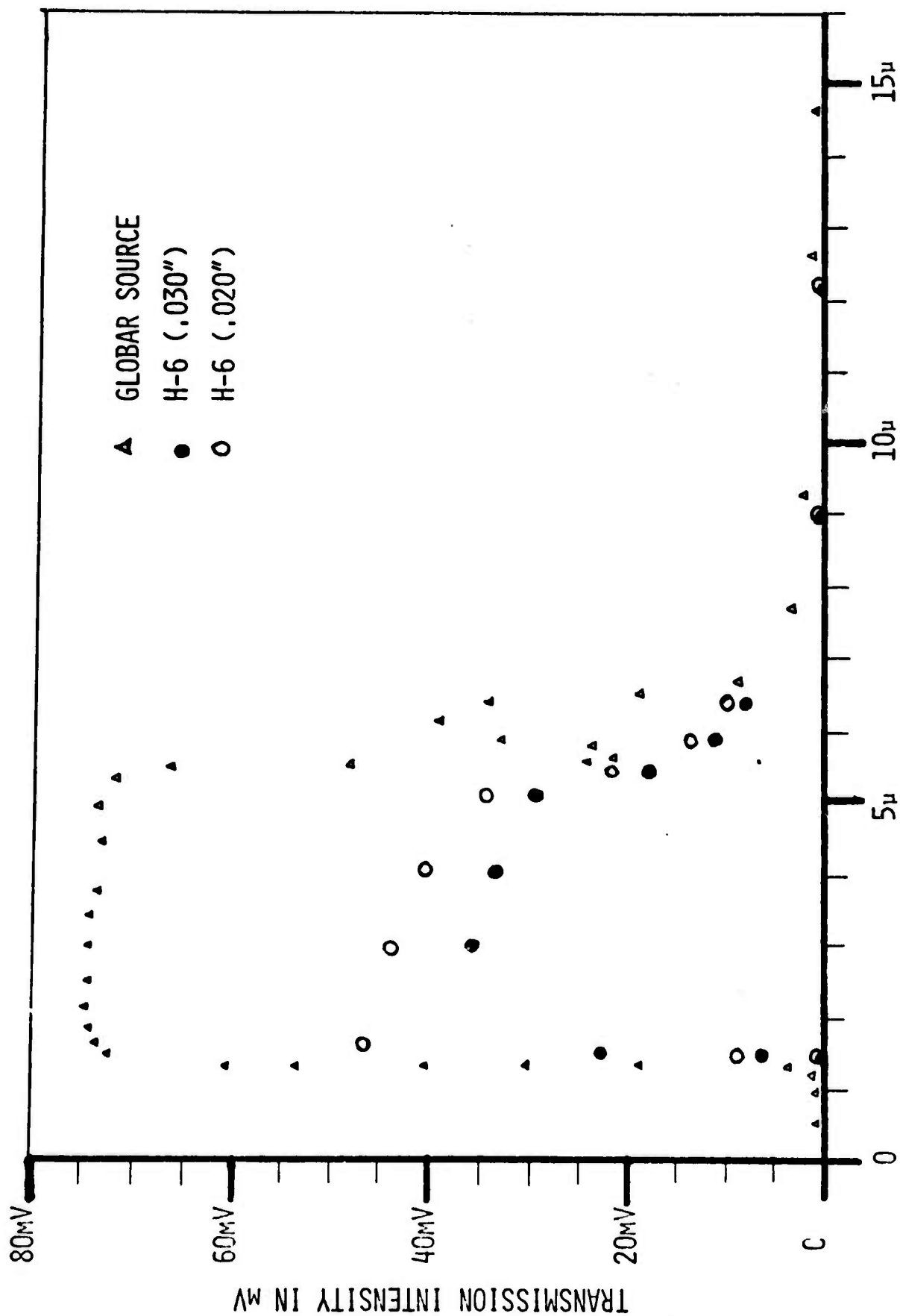


Fig. 19 Transmission intensity versus wavelength for sample H-6 with two different thicknesses.

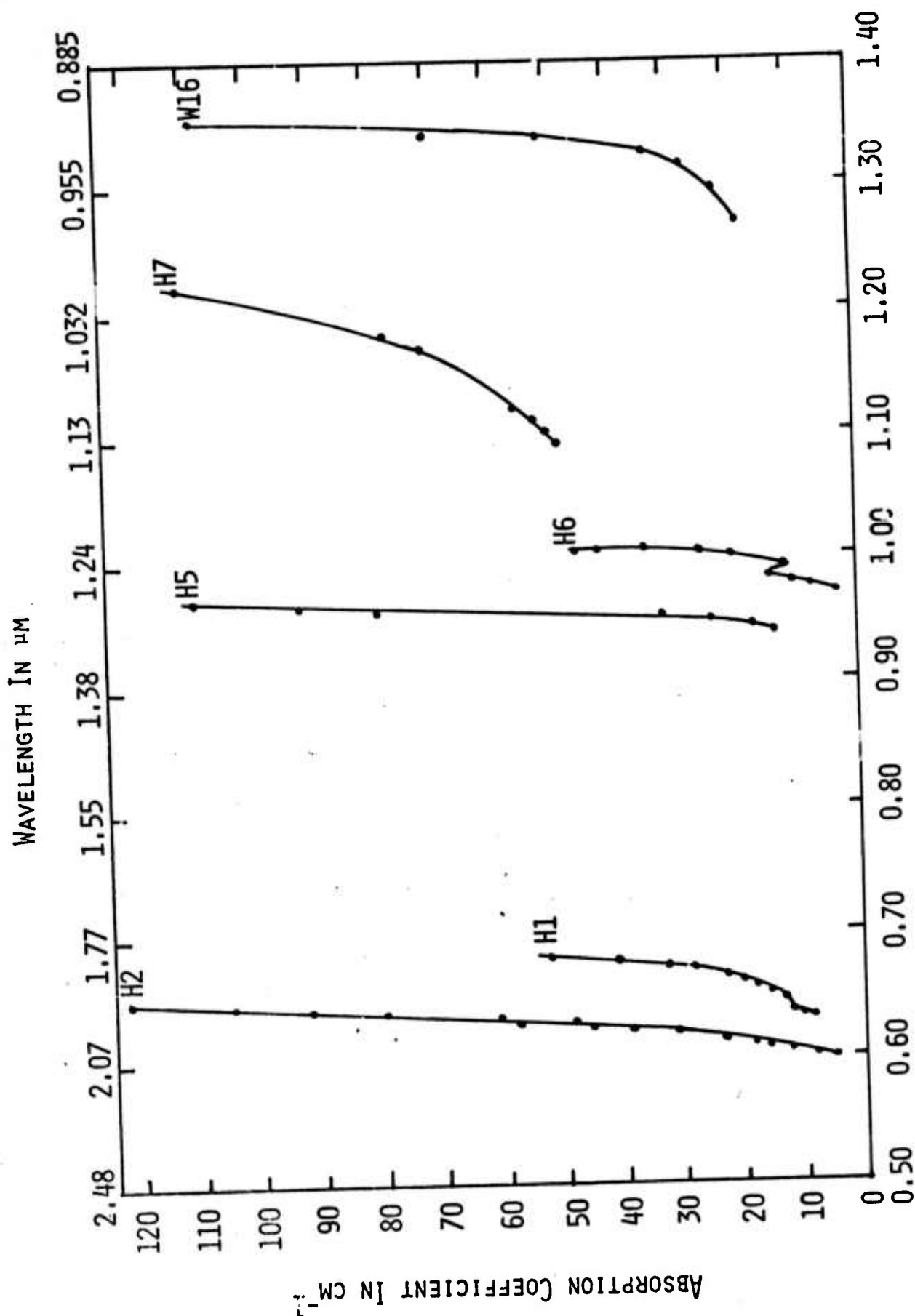


FIG. 20 ABSORPTION COEFFICIENT VERSUS PHOTON ENERGY FOR SAMPLES H-1, H-2, H-5, H-6, H-7 AND W-16.

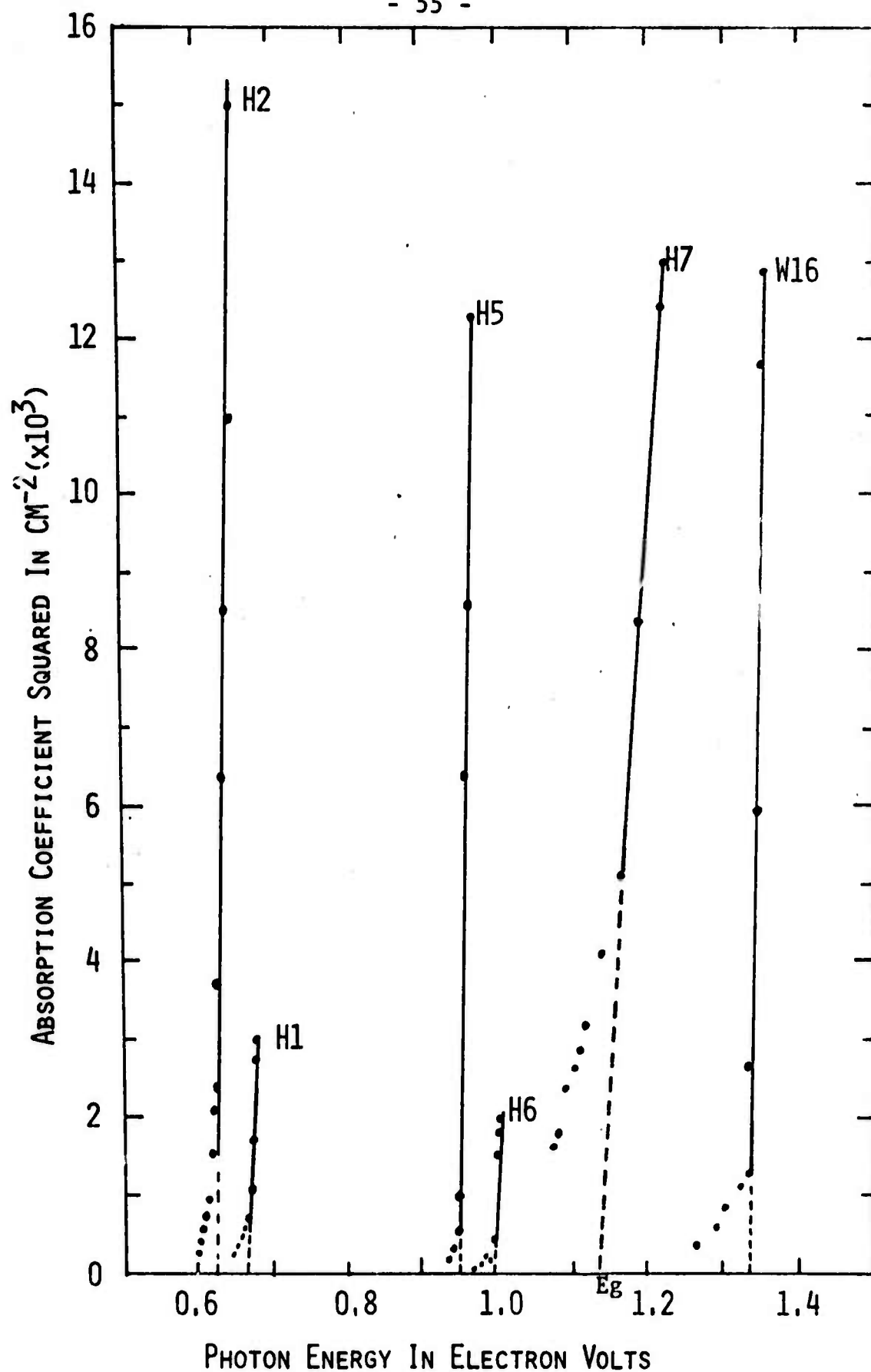


FIG. 21 SQUARE OF THE ABSORPTION COEFFICIENT VERSUS PHOTON ENERGY FOR SAMPLES H-1, H-2, H-5, H-6, H-7 AND W-16.

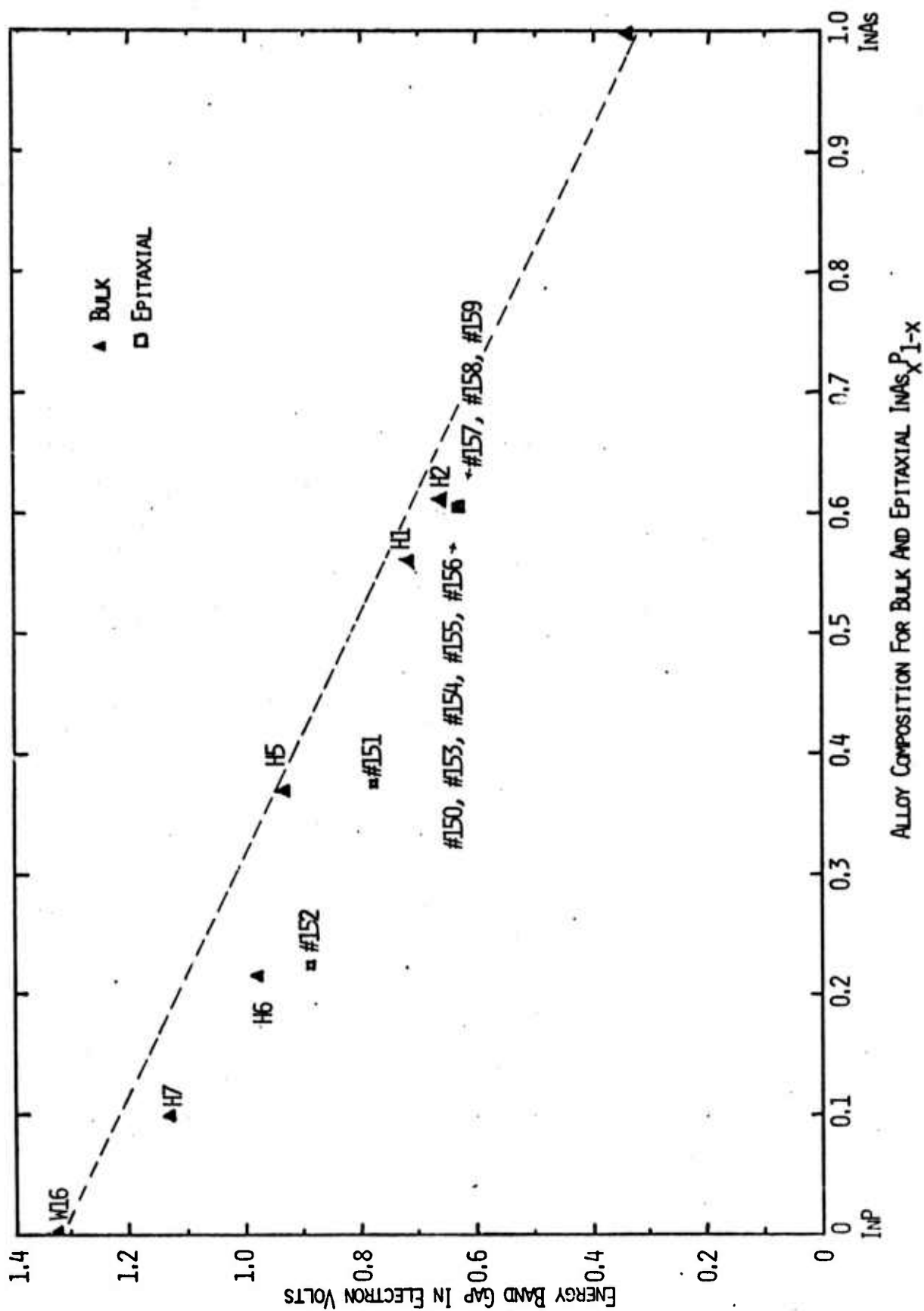


Fig. 22 Energy Band gap versus alloy composition for both bulk and epitaxial $\text{InAs}_{1-x}\text{P}_x$.

V. ANALYSIS OF RESULTS

5.1 Scattering Mechanisms and Electron Mobilities

From the electron mobility data presented in Chapter 4 for the bulk and epitaxial InAsP samples, it is clearly demonstrated that the electron mobility in these specimens is dominated by the polar optical mode phonon scattering for $T > 200^\circ\text{K}$ and by the ionized impurity scattering for $T < 100^\circ\text{K}$. A combined expression for the reciprocal electron mobility can be written as

$$\mu^{-1} = \mu_0^{-1} + \mu_I^{-1} \quad (5-1)$$

where μ_0 is the electron mobility due to polar optical mode scattering, and μ_I is the electron mobility due to ionized impurity scattering.

5.1.1 Ionized impurity scattering

The mobility due to ionized impurity scattering can be calculated by using Brook-Herring equation⁺, which has the reduced form

$$\mu_I = \frac{3.2 \times 10^{15} (m_0/m^*)^{1/2} \epsilon_s^2 T^{3/2} (N_A + N_D)^{-1}}{\ln [1.3 \times 10^{14} T^2 \epsilon_s (m^*/m_0) (N_D - N_A)^{-1}]} \quad (5-2)$$

where, ϵ_s is the relative dielectric constant of the materials, m^*/m_0 is the effective mass ratio, N_D and N_A are donor and acceptor densities, respectively.

In order to calculate the theoretical value of electron mobility from Eq. (5-2), we assume a linear relationship

between ϵ_s and alloy composition, x , and m^*/m_0 and x . Knowing m^*/m_0 and ϵ_s for InP and InAs, we can then compute m^*/m_0 and ϵ_s for $\text{InAs}_{1-x}\text{P}_x$ of any alloy compositions. Table VI lists the effective mass ratio and dielectric constant of some $\text{InAs}_{1-x}\text{P}_x$.

TABLE VI

Relative Dielectric Constant and Effective Mass Ratio
Versus Alloy Compositions for Some $\text{InAs}_{1-x}\text{P}_x$

Material	ϵ_s	m^*/m_0
InP	10.9	0.062
$\text{InAs}_{0.6}\text{P}_{0.4}$	11.1	0.041
$\text{InAs}_{0.8}\text{P}_{0.2}$	11.3	0.034
InAs	11.5	0.027

Knowing $(N_D + N_A)$ and $(N_D - N_A)$ from electron concentration versus temperature plot, one can then calculate the theoretical value of electron mobility from (5-2) for ionized impurity scattering. On the other hand, if μ_I is taken from the experimental data, then N_D and N_A can be calculated from the formula given above.

5.1.2 Polar optical phonon scattering

Scattering of carriers by polar optical mode phonons is of greater importance in compound semiconductors than in the element semiconductors. The relative movement of the two different kind of atoms causes a polarization of the crystal, and a strong interaction with the electrons may result. Our experimental results for bulk and epitaxial InAsP samples clearly show that polar optical mode phonon scattering dominates for temperatures higher than 200°K and the electron mobility is limited by such scattering process. An analysis has been given by Howarth and Sondheimer⁽⁶⁾, and Ehrenreich⁽⁷⁾ has modified their theory to allow for non-parabolic bands. The electron mobility due to polar optical mode scattering is given by⁽⁶⁾

$$\mu_0 = 1.7 \times 10^{30} \left(\frac{e}{e^*}\right)^2 \left(\frac{m_0}{m^*}\right)^{3/2} T^{1/2} Mv \left(\frac{\omega_\ell}{2\pi}\right) F\left(\frac{\theta_\ell}{T}\right) [\exp(\theta_\ell/T) - 1] \quad (5-3)$$

where e^* is the effective charge defined by Callen*, M , reduced mass of the atoms $(= M_1 M_2 / M_1 + M_2)$ and v the volume of the unit cell. $F(\theta_\ell/T)$ is a slowly varying function which decreases from unity at high temperatures to a minimum of 0.6 when $T \approx \theta_\ell$, and then increases

*H. B. Callen, Phys. Rev., 76, 1394 (1947)

steadily with θ_{ℓ}/T , being equal to $0.375\sqrt{(\pi\theta_{\ell})/T}$ at low temperatures. ω_{ℓ} is the longitudinal fundamental optical frequency.

From Eq. (5-3), it is noted that for polar optical mode scattering, the electron mobility should increase exponentially with decreasing temperatures. This is indeed the case for all the InAsP samples studied during this research period, evidenced for temperatures above 150 ~ 200°K. The electron mobilities at 300°K calculated from Eq. (5.3) and the experimental values for InAs, InP and InAs_{1-x}P_x alloys are summarized in Table VII.

5.2 Donor and Acceptor Impurity Densities

From the temperature dependence of the electron concentration (i.e., $\log n$ versus $\frac{1}{T}$ plot) one can usually deduce the material parameters such as donor and acceptor impurities density, the ionization energy of donors and acceptors. For a partially compensated n-type semiconductor (i.e., $N_D \gg N_A$) such as the one studied in this report, the semiconductor statistics provides the following general expression for the electron density

$$n = \frac{2(N_D - N_A)}{[1 + (\frac{N_A}{gN_C}) \exp(\frac{E_C - E_D}{kT})] + [1 + \frac{N_A}{gN_C} \exp(\frac{E_C - E_D}{kT})]^2 + \frac{4(N_D - N_A)}{gN_C} \exp(\frac{E_C - E_D}{kT})}^{1/2} \quad (5-4)$$

where N_D and N_A are the donor and acceptor density, respectively, $N_D = 2(\frac{2\pi m^* kT}{h^2})^{3/2} = 2.5 \times 10^{19} (T/300)^{3/2}$ is the effective density of conduction band states, and g is degenerate factor; $g = 2$ for the ground donor state with single spherical energy surface.

E_D is the donor energy level measured from the conduction band edge.

At low temperatures in which $n \ll N_A < N_D$, Eq. (5-4) reduces to

$$n \approx (\frac{N_D - N_A}{N_A/g}) N_C \exp(-\frac{E_C - E_D}{kT}) \quad (5-5)$$

The quantity $(N_D - N_A)$ is readily determinable from the high-temperature exhaustion range of the $\log n$ vs. $\frac{1}{T}$ plot, and the slope of this curve would yield the donor ionization energy.

Eqs. (5-4) and (5-5) are used to compute the donor and acceptor densities, the ionization energy of the donor state in the $\text{InAs}_{1-x}\text{P}_x$ samples. From $\log n$ versus $\frac{1}{T}$ plot for bulk and epitaxial $\text{InAs}_{1-x}\text{P}_x$ samples shown in Chapter 4 we were able to calculate both N_D and N_A as well as E_D for each sample. The value of $(N_D - N_A)$ was obtained at 3°K in which a plateau was observed. The calculated value for N_D , N_A and E_D as well as other pertinent parameters for the InAsP samples are summarized in Table VIII.

5.3 Impurity Hopping Conduction at Low Temperatures

It is obvious from the experimental results on bulk and epitaxial InAsP samples that the impurity hopping conduction process dominates at low temperatures ($T < 10^\circ\text{K}$) for all samples studied during this contract period. This is due to fact that these samples are moderately or highly compensated and as a result the electrons are able to conduct by hopping through partially emptying donor states at extremely low temperatures. Conwell⁽⁸⁾ first derived a model for dc hopping conductivity. Considerable amount of work has been done since then.⁽⁹⁻¹⁰⁾ Consider a donor concentration N_D (total), of which N_D^+ are donors without a bound electron as a result of partial compensation. An electron bound to one donor can tunnel over to an adjacent empty one. The impurity band resistivity for hopping conduction is given by⁽⁸⁾

$$\rho \approx \left(\frac{h k T}{16 \epsilon_s E_{act}} \right)^2 \left(\frac{N_D}{N_D^+} \right) \exp \left(\frac{2 r_s}{\epsilon_s a_H^*} \right) \quad (5-5)$$

Which predicts that for impurity band hopping conduction, the resistivity ρ varies linearly with temperatures.

Figure 23 and 24 show this dependence for epitaxially grown $\text{InAs}_{0.61}\text{P}_{0.39}$ samples and bulk samples H-2 and H-6 for $T \leq 20^\circ\text{K}$.

Table VII
Calculated and Experimental Mobilities For
InAs_{1-x}P_x at 300°K

Material	Carrier	m^*/m_0	e^*/e	$\omega_L \times 10^{13} (\text{sec}^{-1})$	$\theta_L (^\circ\text{K})$	Polar Mobility ($\text{cm}^2/\text{V-S}$)	Observed Mobility	Remarks
InAs	Electron	0.027	0.22	4.4	340	40,000	33,000	Ref. (8)
InP	"	0.062	0.24	0.6	480	6,800	4,600	Ref. (8)
H-2	"	--	--	--	--	--	4,200	present work
H-5	"	--	--	--	--	--	42,000 (?)	"
H-6	"	--	--	--	--	--	4,100	"
153-159	"	0.041	0.23	3.35	256	4,000	3,700	"

Table VIII Donors and Acceptors Density, Activation Energy of Donor States for Epitaxial InAs_{0.61}P_{0.39} Samples (300°K)

Sample No.	$(N_D - N_A) (\text{cm}^{-3})$ $\times 10^{16}$	$N_D (\text{cm}^{-3})$ $\times 10^{16}$	$N_A (\text{cm}^{-3})$ $\times 10^{16}$	N_A/N_D	$E_D (\text{eV})$
InAs _{0.61} P _{0.39}					
153	4.23	4.71	.48	.102	.0146
154	4.84	5.78	.94	.163	.0148
155	7.96	11.48	3.52	.307	.0100
156	4.76	5.06	0.30	.0593	.0095
157	4.85	6.45	1.60	.248	.0100
159	5.25	7.25	2.00	.276	.00404
H2	4.55	4.97	0.42	.084	.0048

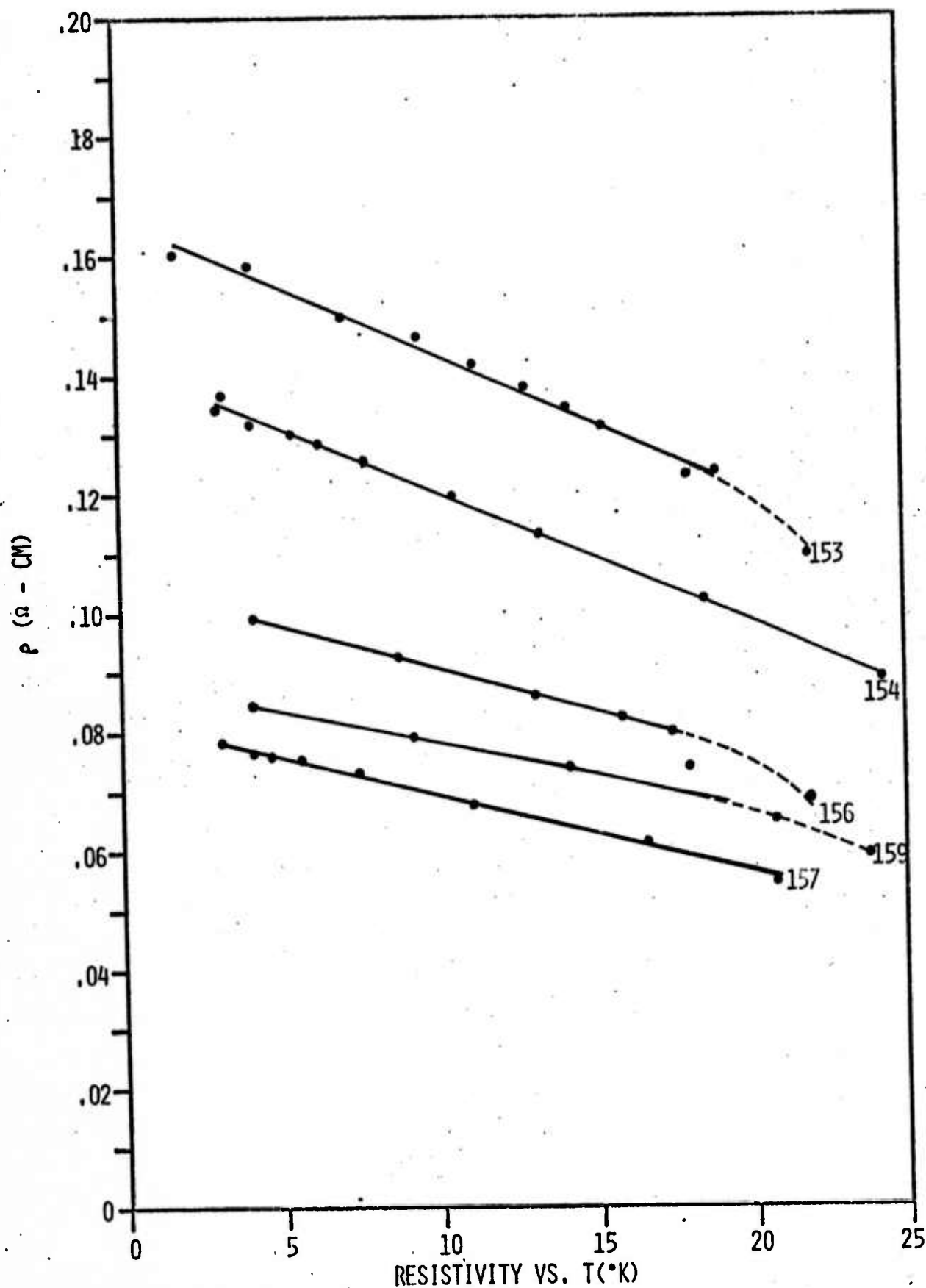


Fig. 23 Resistivity versus absolute temperature for epitaxial samples 153, 154, 156, 157 and 159 for $3^{\circ}\text{K} < T < 25^{\circ}\text{K}$.

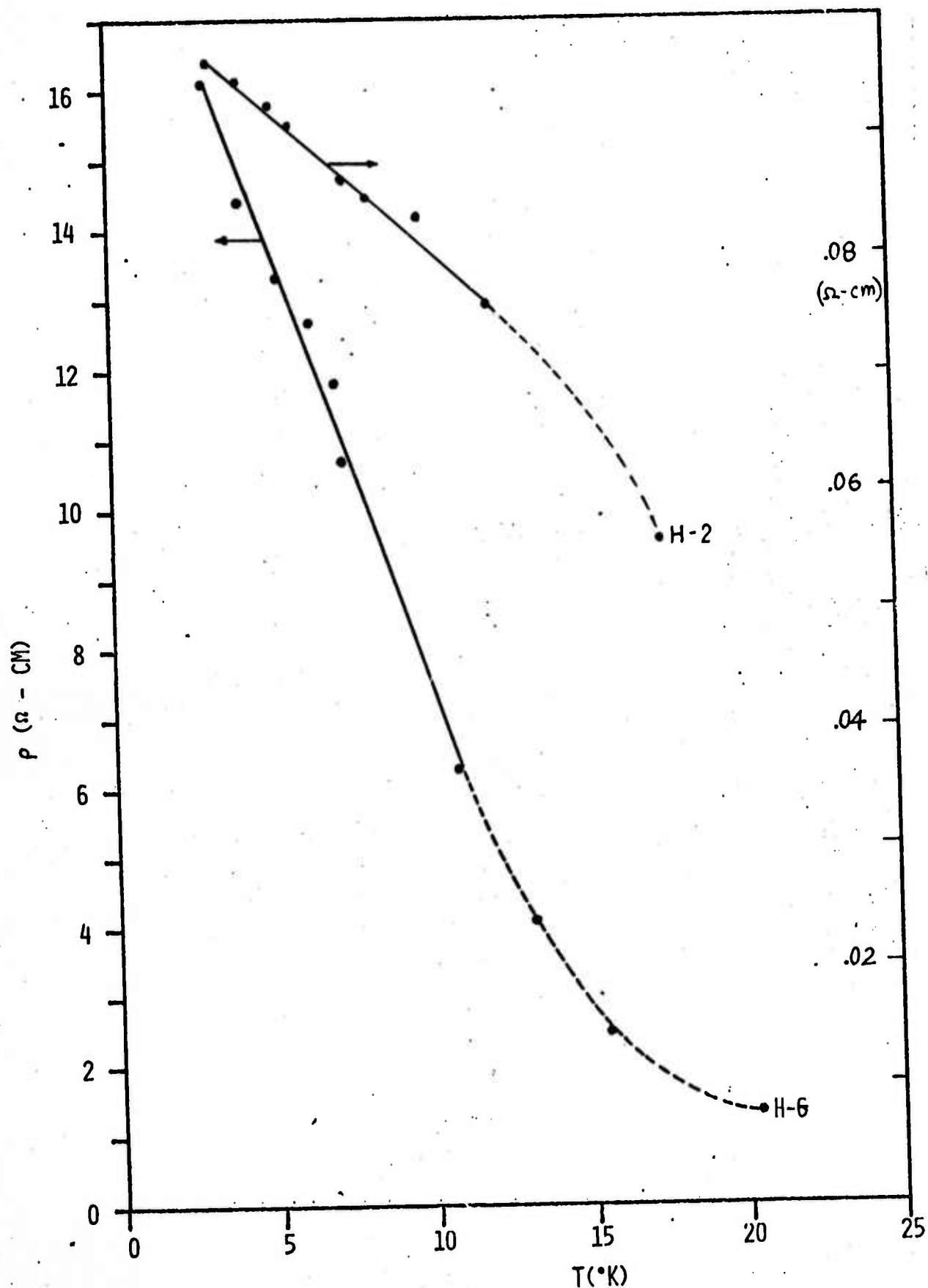
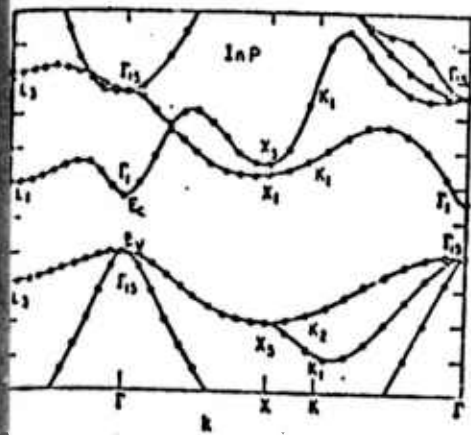


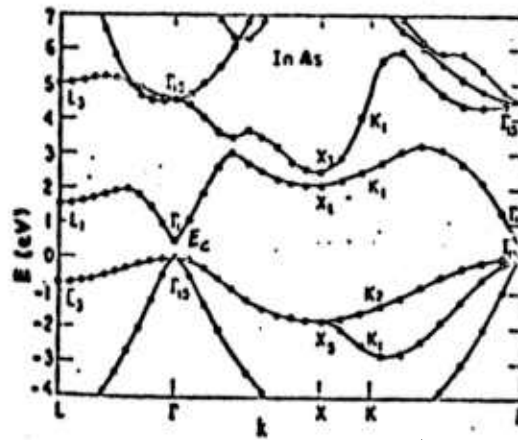
Fig. 24 Resistivity versus absolute temperature for bulk samples H-2 and H-6 for $3^{\circ}\text{K} < T < 20^{\circ}\text{K}$

5.4 Energy Band Structure For InAs, InP and $\text{InAs}_{1-x}\text{P}_x$

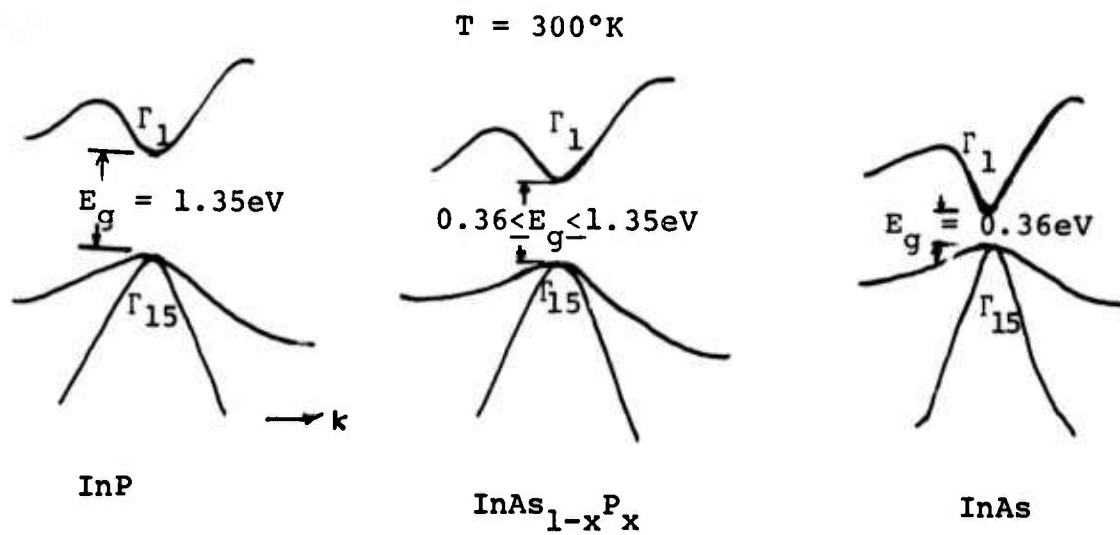
InAs and InP are known to be the direct band gap semiconductors with both conduction band minimum and valence band maximum occurring at Γ point in k-space (see Fig. 25). Room temperature energy gap for InP is $E_g = 1.35$ eV and $E_g = 0.34$ eV for InAs. The change in alloy composition x in the $\text{InAs}_{1-x}\text{P}_x$ alloy system will modify the band structure of the InAs and InP. Results of optical absorption coefficient squared α^2 versus photon energy, $h\nu$ show that these alloys are direct gap semiconductors. This result confirmed that the change in alloy composition will alter the energy band gap at Γ point. From optical absorption data taken at the fundamental absorption edge and the electron microprobe analysis, it was found that the energy band gap varies approximately linear with the alloy compositions of $\text{InAs}_{1-x}\text{P}_x$ as was illustrated in Fig 22. The proposed band structure for $\text{InAs}_{1-x}\text{P}_x$ alloy system is shown in Fig. 25 along with the band structures for InAs and InP.



(a) InP



(b) InAs



(c)

FIG. 25 Energy band Structure for InAs, InP, and $\text{InAs}_{1-x}\text{P}_x$

5.5 Summary

Discussions and analysis have been given in this chapter concerning scattering mechanisms (polar optical mode scattering and ionized impurity scattering), donor and acceptor densities and ionization energy, impurity hopping conduction mechanism and the energy band structure of the $\text{InAs}_{1-x}\text{P}_x$ alloy system. It has been shown that experimental results (i.e., resistivity, Hall effect, optical transmission and electron microprobe measurements) support the general picture of the theoretical analysis described in this chapter. The present study leads to the following conclusions concerning the general transport and optical properties of $\text{InAs}_{1-x}\text{P}_x$ system:

- (a) Electron mobilities in bulk and epitaxial $\text{InAs}_{1-x}\text{P}_x$ samples are limited by polar optical mode scattering for $T > 200^\circ\text{K}$ and ionized impurity scattering for $T < 100^\circ\text{K}$. Good agreement was obtained between theory and experiment.
- (b) From Hall effect measurement, it was found that the density of donors in these samples is in the order of 10^{16}cm^{-3} . The compensation of N_D and N_A in most of the samples studied is considerably high, although some samples show light compensation.
- (c) The normal band conduction prevails for $T > 50^\circ\text{K}$ while impurity hopping conduction process dominates for $T < 15^\circ\text{K}$.

- (d) Optical absorption data and electron microprobe analysis leads to the conclusion that energy band gap varies approximately linear with alloy composition.

VI. FUTURE PLANS

Results obtained during this contract period provide us with a general understanding of the basic electronic transport and optical properties in the InAsP alloy system. Useful information and physical parameters such as electron mobilities, donor and acceptor densities, activation energy of donor states, optical absorption coefficient, scattering mechanism and energy band structure for InAsP have been obtained from this study. A continuous effort will be made in the third and fourth quarter of this research contract concerning the detailed comparison between theory and experimental results on the electron mobility and other physical parameters. Extensive studies will be conducted on the effect of changing the growth conditions (i.e., H_2 flow rate, epitaxial thickness and substrate orientation) on improving the purity of epitaxial layers. In addition to our present efforts, we will start working on optical reflectance measurement, photoluminescence experiment, photoconductivity decay experiment and thermally-stimulated current measurements to study shallow impurity and defect energy states, lifetimes and trap energy levels in InAsP alloy systems.

REFERENCES

1. H. Fritzche, J. Phys. Chem. Solids, vol. 6, pp. 69-80 (1958).
2. R. J. Sladek, J. Phys. Chem. Solids, vol. 5, pp. 157-170 (1958).
3. A. G. Thompson and J. W. Wagner, J. Phys. Chem. Solids, vol. 32, pp. 2613-2619 (1971).
4. van der Pauw Phillip Research Report (1956).
5. O. Lindberg, Proc. I.R.E., vol. 40, 1414 (1952).
6. D. J. Howarth and E. H. Sondheimer, Proc. Roy. Soc., A219, 53 (1953).
7. H. Ehrenreich, J. Phys. Chem. Solids, vol. 12, pp. 97-104 (1959).
8. E. M. Conwell, Phys. Revs., 103, 51 (1956).
9. N. V. Zotova, T. S. Lagunova, and D. N. Nasledov, Sov. Phys. Solid States, vol. 5, 2439 (1964).
10. F. P. Kesamanly, et al., Sov. Phys. Solid State, vol. 6, 741 (1964).

OTHER REFERENCES

1. von O. G. Folberth, "Mischkristallbildung bei A^{III}-B^V-Verbindungen," Z. Naturforschg. 10a, 502-503 (1955).
2. von H. Weiss, "Über die Elektrischen Eigenschaften von Mischkristallen der Form $\text{In}(\text{As}_{1-x}\text{P}_x)$," Z. Naturforschg. 11a, 430-434 (1956).
3. H. Ehrenreich, "Electron Mobility of Indium Arsenide Phosphide," J. Phys. Chem. Solids, vol. 12, pp. 97-104, (1960).
4. A. G. Thompson and J. W. Wagner, "Preparation and Properties of $\text{InAs}_{1-x}\text{P}_x$ Alloys," J. Phys. Chem. Solids, vol. 32, pp. 2613-2619 (1971).
5. J. J. Tietjen, J. P. Maruska and R. B. Clough, "The Preparation and Properties of Vapor-Deposited Epitaxial $\text{InAs}_{1-x}\text{P}_x$ Using Arsine and Phosphine," J. Electrochem. Soc., pp. 492-494 (April 1969).
6. H. A. Allen and E. W. Methal, "Deposition of Epitaxial $\text{InAs}_{1-x}\text{P}_x$ on GaAs and GaP Substrates," J. Electrochem. Soc., vol. 117, pp. 1081-1082 (1970).
7. F. B. Alexander, et al., "Spontaneous and Stimulated Infrared Emission from InPAs Diodes," Appl. Phys. Letter, vol. 4, pp. 13-15 (1964).
8. Bernd Ross, "Properties of InAsP Lasers," J. of Electrochem. Soc., 94C (March 1970).
9. K. Graff and H. Pieper, "Bestimmung Der Zusammensetzung Von Ternären III-V-Verbindungshalbleitern aus dem Spectrum der Oberflächenfotospannung," Solid State Electronics, vol. 15, pp. 831-837 (1972).
10. J. R. Buckmelter and J. K. Kennedy, "Electron Microprobe Characterization of Vapor-phase Grown $\text{InAs}_{1-x}\text{P}_x$ Layers," J. Electrochem. Soc., vol. 120, p. 133 (1973).